COMPUTATIONAL MODEL FOR STEADY STATE SIMULATION OF A SOLID OXIDE FUEL CELL (SOFC) PLANAR STACK MODEL UNDERGOING REFORMING PROCESS

by

VAIBHAV VIJAY INDULKAR

Presented to the Faculty of the Graduate School of

The University of Texas at Arlington in Partial Fulfillment

of the Requirements

for the Degree of

MASTER OF SCIENCE IN MECHANICAL ENGINEERING

THE UNIVERSITY OF TEXAS AT ARLINGTON

DECEMBER 2017

ACKNOWLEDGEMENTS

I would like to thank Dr. Daejong Kim for his guidance, encouragement, and constant support during the entire research work at University of Texas at Arlington. I deeply thank him for giving me the opportunity to work at Turbomachinery and Energy System Laboratory at University of Texas at Arlington. His vision and dedication towards work will always be a source of inspiration for me. I sincerely express my gratitude to Dr. Ankur Jain and Dr. Albert Tong for kindly accepting to be members of the supervising committee.

I would like to thank Ajit Desai, Amirreza Niazmand, Srikanth Hanovara-Prasad, Myongsok Song and all my fellow colleagues at Turbomachinery Energy System Laboratory for their guidance and support.

Finally, I thank my family for their constant support and belief, encouraging me attain my career goals.

December 11, 2017

ABSTRACT

COMPUTATIONAL MODEL FOR STEADY STATE SIMULATION OF A SOLID OXIDE FUEL CELL (SOFC) PLANAR STACK MODEL UNDERGOING REFORMING PROCESS

Vaibhav Vijay Indulkar, M.S.

The University of Texas at Arlington, 2017

Supervising Professor: Daejong Kim

Solid Oxide Fuel Cell (SOFC), is a clean and low-pollution technology of generating power of high efficiency. Its applicability for both stationery and transportation power generation systems, adaptability for wide range fuel sources, as wells its process of direct conversion of fuel to energy make it an important source of power generation. An effective design of sub-systems or individual components play a key role in overall working of a plant. Thus, critical analysis at the component level is of importance for the overall plant efficiency. In the present study a heat transfer model of a planar SOFC stack to be used as a component in a hybrid gas turbine power generation system is analyzed. The planar stack model is studied owing to its advantage in terms of high output power density, applicability for wide power generation systems, ease in component level design and manufacturing. The thesis presents a numerical heat transfer model in which a finite volume computational technique is used to solve the governing energy equation for fluid flow and heat transfer. Convection-diffusion equation is used to model the temperature variation for air and the fluid mixture. Heat conduction equation to model temperature variation through the metal structure. Thermodynamic species balance to model species variation in the mixture owing to steam reforming and water gas shift reaction occurring in the stack. Property variation for air and

gas mixtures like specific heat, viscosity, conductivity, mixture concentration and reaction kinetics like Gibbs energy, reaction rate, rate constant, equilibrium constant are modelled as a function of temperature. Flow admittance form of the momentum equation is used to model momentum. The solver thus solves for the temperature for air, gas mixture, solid geometry, and the concentration of the species iteratively till all the values converge. The model can be easily integrated into a hybrid cycle called as “SOFC Gas-Turbine Hybrid System” or can be used as a stand-alone model to simulate the stack at component level.

TABLE OF CONTENTS

LIST OF ILLUSTRATIONS

LIST OF TABLES

Chapter 1

INTRODUCTION

1.1 Background

The demand for power generation systems of high efficiency with low emission is an ever-increasing trend. Environmental problems such as global warming and its adverse effect has put more emphasis on reducing the usage of fossil fuel and thereby encouraged researchers to put focus on development of efficient and clean power generation systems. In view of these Fuel cells as an alternative to conventional energy conversion system have proved to be more efficient and environment friendly power generation source. This has led to the applications of Fuel Cell Technology to various field such as automobiles, stationery power generation systems etc.

Comparing to other power generation system such as heat engines where chemical energy is first transformed into thermal energy, then to shaft work by combustion process and finally to electric power, Fuel Cell transforms chemical energy directly to electric power in a single efficient step. The cell is supplied with hydrogen rich fuel with undergoes oxidation process to produce electricity and exhaust. The exhaust mostly consists of steam which can be recirculated within the plant which in turn increases the system overall efficiency. While the modern power generation system reaches 40% low heating value efficiency(LHV) the Fuel Cell Engines operate at the efficiency of around 45% [3]. As a result, they can be used in small applications called as “distributed power generation system” or can be combined with the gas turbines in hybrid large scale power generation called as “SOFC Gas Turbine Hybrid Power Generation System”.

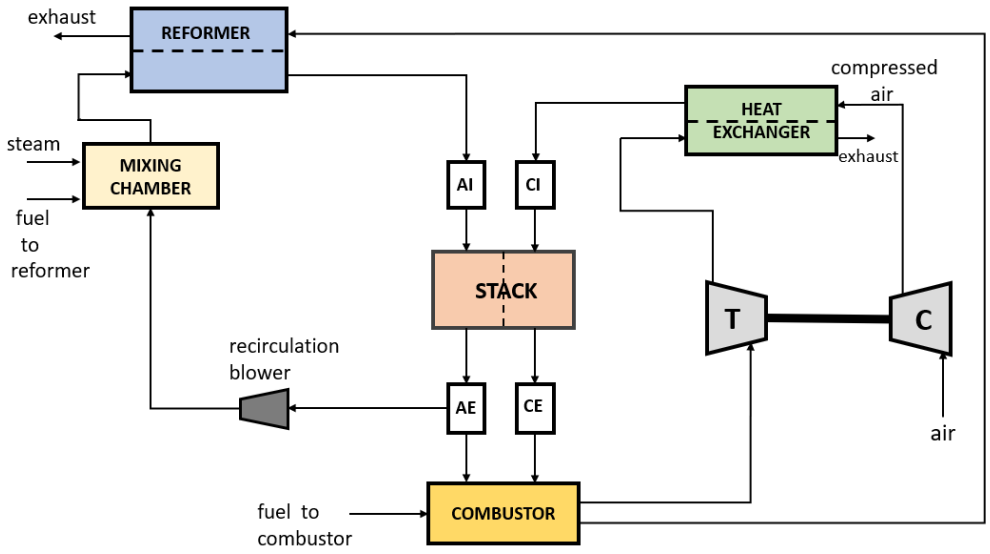

Figure 1-1 SOFC Integrated GT- Cycle

The Figure 1.1 represents a SOFC integrated GT-cycle, the advantage of integrating/hybridizing the SOFC with gas turbine is to increase the performance of the SOFC by using the turbine as a source for hot air supply to the cathode of the SOFC. The combination results in an efficient means of generating electric power rather than using an external power supply to heat the incoming air to the cathode channel of the SOFC stack [2]. The cycle consists of a stack, combustor, reformer, heat exchanger, compressor, and a turbine. In the above figure AI and CI represent the anode and cathode inlet respectively, whereas AE and CE represent the exit for the anode and the cathode. The starting point of the cycle is the combustor where external fuel is supplied and burned with excess air exiting the cathode of the SOFC stack, the thermal energy generated is used to heat the heat exchanger, reformer and stack at the required start-up temperature [1]. The above components should be heated initially to the operating temperature for the efficient working of the cycle. The gases leaving the combustor serves two purposes. Firstly, to heat up the compressed air delivered by the compressor to a high temperature through a heat

exchanger. Secondly, in the reforming process of the fuel mixture entering the reformer. The high temperature air leaving the heat exchanger enters the cathode side of the stack. Once the components reach the operating temperature the fuel and steam mixture are supplied to reformer to undergo reforming. The reformed hydrogen rich gas enters the stack through the anode inlet where electro-chemical reaction occurs generating electrical power. The unreformed fuel from the reformer is further reformed in the stack by the hot air entering the cathode, this is called as internal reforming. Once the cycle starts the external supply of the steam to the mixing chamber is cut and the excess unreacted steam from the anode exhaust of the stack is recirculated to the mixing chamber using the recirculation blower. A continuous operation of combustor is essential to continuously burn the non- reacted fuel, also external fuel and air supply is provided to maintain the air to fuel ratio [18]. As can be seen a careful designing of all the components is necessary to maintain balance of plant (BOP) in turn reducing the operating cost of the entire cycle.

1.1.1 Background of SOFC

There are different types of fuel cell available such as Proton Exchange Membrane(PEM), Alkaline Fuel Cell (AFC), Phosphoric Acid Fuel Cell (PAFC), Molten-Carbonate Fuel Cell(MCFC), Direct Methanol Fuel Cell(DMFC), Solid Oxide Fuel Cell (SOFC) etc. All the above fuel cells work at different temperature and pressure conditions with different fuel supply, design, and material. Among all the mentioned types the SOFC is recognized to be efficient and robust for stationery power generation system. SOFC works at the high temperature range usually 600~700 ℃. It can be coupled with gas turbine(GT), heat exchanger, reformer etc. to achieve high performance efficiency. Moreover, due to synergistic effect hybridization of SOFC with gas turbine has been proved as a superior technology for power generation. Predicted results have shown that integration of

pressurized SOFC into complex GT system, with multistage, inter-cooler, heat exchanger can result into electrical efficiency of 70% or higher [2].

Hydrocarbon such as methane, propane can be directly used as fuel unlike other fuel cell which need pure hydrogen for their operation this is most attractive feature of SOFC. The cells are fed with hydrogen rich fuel in the gaseous form. Pure hydrogen is avoided because of low density, high flammability and volatility which makes handling difficult. Low density increases storage cost for the fuel. Generally, three sources are considered for hydrogen production like electrolysis, reforming and from biogas production of which hydrogen obtained from reforming process is the most reliable method [3]. The high working temperature allows for improved internal reforming of fuel, chemical activities and charge transport as a result, the overall system efficiency increases. In the cell, at the interface on the cathode side where the electrode, electrolyte and cathode gas meet the reduction reaction of oxygen occurs releasing oxygen ions which pass through the electrolyte to enter the anode side. At the anode interface where the electrode, electrolyte and anode gas meet, the oxygen ions react with hydrogen to form water and release electron which then pass through the anode electrode and to the external load.

The Figure 1.2 and the chemical reactions mentioned explains the process occurring inside a cell.

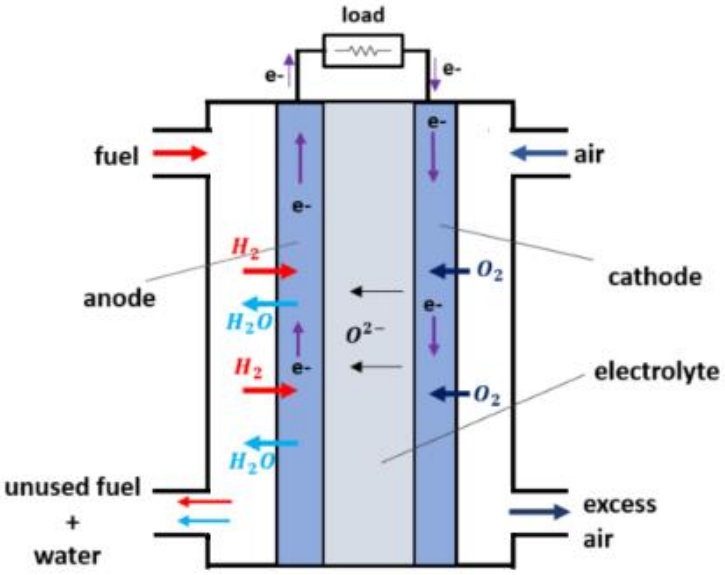

Figure 1-2 Diagrammatic representation of the cell

The two electrochemical half reactions in a SOFC are,

$$\frac{1}{2}O_2 + 2e^- \rightarrow O^{2-} \quad (cathode\ reaction)$$

$$H_2 + O^{2-} \rightarrow H_2O + 2e^- \quad (anode\ reaction)$$

On cathode side, oxygen reduction reaction occurs releasing oxygen ions. These oxygen ions carry charge across the ion conducting electrolyte to the anode where they react with hydrogen to produce water and release electrons. These released electrons travel through the electron conducting phase to the external circuit to harness the electrical power.

1.2 Stack models

1.2.1 Tubular model

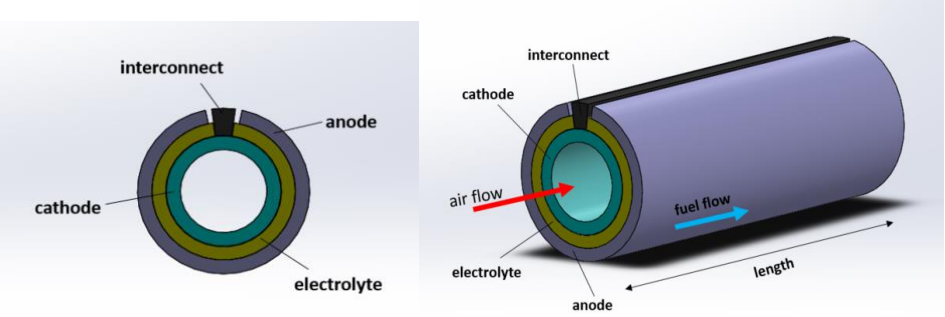

Figure 1-3 Diagrammatic representation of tubular model

The tubular design developed by Siemens Westinghouse is illustrated in Figure 1-3. The components (hardware) are similar in both the tubular as well as in the planar design i.e. cathode electrode, anode electrode, electrolyte, interconnect. The inner electrode is a cathode which is usually doped lanthanum manganite tube. The electrolyte used is Yttria-Stabilized-Zirconia (YSZ) which is deposited over the cathode. The outer most layer is anode made of Ni/YSZ. The interconnect which runs as strip along the length of the cell is made of doped lanthanum chromite [4]. Hot air passes through the inner tube from a supply whereas the fuel is delivered through the outermost tube. Compared to the planar design the tubular model is sealant free which increases its thermal stability which serves as a major advantage. However, there are high ohmic and electrical losses associated with the tubular model owing to the long path the electrons must follow along the length of the design thus affecting the output and contributing as a major disadvantage compared to planar design [1]. The power density of tubular design is around 0.2 to 0.25 W/cm^2 at about 1000 ℃ which is considerably low compared to planar design which is high around 2 W/cm^2.

1.2.2 Planar model

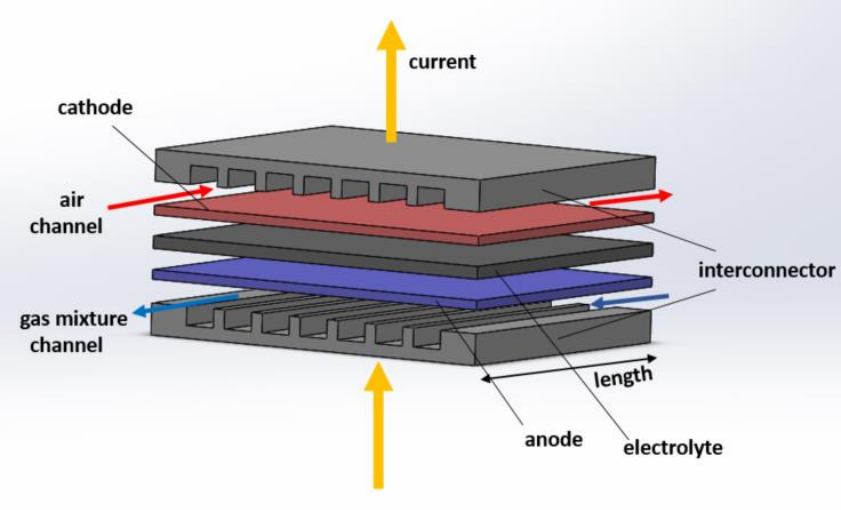

Figure 1-4 Diagrammatic representation of the planar model

As discussed in the section 1.2.1, due to low power density of the tubular model compared to that of the planar design, the tubular design can only be used for stationery power generation system. Whereas the planar design can be used for both stationery and transportation power generation systems which serves an advantage over the tubular design. The generic design of the planar SOFC is as above, which shows channel for air and gas mixtures separated by the cathode, electrolyte and anode together called as membrane electrode assembly (MEA). Adjacent cells are connected using interconnect. The hardware design can be counter-flow, parallel-flow or a cross-flow depending on the requirement, application and can be customized as needed. The material used for construction is mentioned in section 1.2.3. In the present thesis, the planar model is analyzed, and a deep insight can be obtained about the working of the model in this work.

1.2.3 Components of SOFC

Electrolyte

The electrolyte is a thin ceramic membrane that allows transport of ions. The common electrolyte used are Yttria-Stabilized-Zirconia (YSZ), Mg-doped lanthanum gallate (LSGM), and Gadolinium (Gd) or Sm-doped ceria (CGO or CSO). The electrolyte should have high ionic conductivity, low electron conductivity, stability over long period of operations. Apart from exhibiting above properties the electrolyte provides separation for fuel and oxidant and thus prevent the fuel crossover [1]. YSZ is the most commonly used electrolyte because it allows for sufficient ionic conductivity at high temperature also it exhibit steady electrical and mechanical characteristics at high temperature.

Anode

The anode is the thickest and strongest layer in a cell that provides mechanical support because it has least polarization losses. Fuel oxidation reaction occurs at anode. Ni-YSZ cermet is the most common anode material used. Ni provides good catalytic activity and electronic conductivity while YSZ provides the ionic conductivity [22].

Cathode

The cathode is where the oxygen reduction reaction occurs. The most common cathode material is Strontium-doped lanthanum magnetite (LSM), a semiconductor as it provides sufficient physio-chemical properties, catalytic activity and electrical conductivity. LSM is especially popular at high temperature because losses at the cathode increases significantly as the SOFC temperature is lowered [1].

Interconnect

The interconnect connects two adjacent cells in the arrangement desired i.e. series or parallel connections. It is also called as bipolar plate in planar SOFC model. It can be either metallic or ceramic. I should be highly stable because it exposed to oxidizing and the reducing reaction sides of the cell on either side. Ceramic are better choice compared to metal for long life of the interconnect. However, they are expensive compared to metals. Nickel and steel based alloys are used for lower temperature application. Composite material like Cermet which is combination of ceramic and alloys are under consideration. Chromium metal alloys with good electrical conductivity, mechanical stability and thermal conductivity are also common interconnect materials.

1.3 Reforming

As discussed in the introductory part, the storage and transport of pure hydrogen adds highly to the cost. Reforming of liquid fuel or hydrocarbon at site is the widely accepted practice. The conversion process of hydrocarbon to hydrogen is typically carried out by using the three established processes mentioned below.

Steam reforming (SR)

In SR only fuel and steam are fed into the reactor. The complete SR reaction is highly endothermic and hence requires large amount of heat.

$$CH_4 + H_2O \leftrightarrow 4H_2 + CO_2 \quad \Delta h_f = 165\ kJ/mol$$

It is a combination of two individual reactions, steam reforming(SR) and water gas shifting (WGS). The hydrogen obtained by this process is highest compared to all the three processes because there is no oxygen involved in the reaction process and the outlet hydrogen is free from nitrogen.

$$SR \quad : CH_4 + H_2O \leftrightarrow CO + 3H_2 \qquad \Delta h_f = 206 \ kJ/mol$$

$$WGS \ : CO + H_2O \leftrightarrow H_2 + CO_2 \qquad \Delta h_f = -41 \ kJ/mol$$

Partial oxidation (POX)

In POX fuel and sub-stoichiometric amount of air are fed into the reactor to partially oxidize the fuel mixture to CO and H_2. It is an exothermic reaction. The hydrogen produced is lesser by POX [19].

$$CH_4 + \frac{1}{2}O_2 \rightarrow CO + 2H_2 \qquad \Delta h_f = -36 \ kJ/mol$$

Auto-thermal reforming (ATR)

ATR is a combination of SR and POX carried out in a single reactor. These reactions are simultaneous and uses energy liberated by one reaction for the other to occur.

$$CH_4 + 0.5\lambda(O_2 + 3.79N_2) + (1-\lambda)H_2O \leftrightarrow CO + (3-\lambda)H_2 + 1.895\lambda N_2$$

If $\lambda = 0$ we get SR.

In SR reactions in addition to the reactions mentioned above, the following reactions may occur resulting in carbon formation at the surface of the reactor walls, catalyst and hence degrading the performance by reducing activity [3].

$$CH_4 \rightarrow C + 2H_2$$

$$2CO \rightarrow C + CO_2$$

This phenomenon is controlled by supplying an optimum steam to carbon ratio at the inlet. Previous studies confirm that SCR around 2 to 2.5 can be chosen as an optimum range. Higher value may dilute the hydrogen at the outlet whereas lower SCR may result in carbon formation. Due to endothermic behavior of the SR reaction high thermal energy need to be supplied continuously, these heat is supplied by preheating the mixture using a preheater.

Reforming can be carried out internally inside the cell stack or externally using external reformer. Internal reforming in SOFC can simplify the complexity of the system, However, it can result in thermal gradients inside the cell due high heat interaction resulting in thermal stresses in the electrolytes.

1.4 Thesis Objective

The objective of the thesis is to develop a computational solver to simulate steady state working of a SOFC stack undergoing reforming process. The planar design of the stack is used as a reactor to model the process of fluid flow, heat transfer and chemical kinetics. The model simulates reforming of hydrocarbons to hydrogen by the process of Steam Reforming (SR) and Water Gas Shifting (WGS). The developed solver can be integrated with hybrid GT power cycle or can be used as a stand-alone solver to model the process occurring inside SOFC stack. It can also be used as heat exchanger model by adjusting certain parameters like fluid properties, dimensions (stack or heat exchanger geometry), inlet conditions of temperature and pressure etc.

1.5 Organization of Thesis

The thesis is divided into six major chapters. The initial part of Chapter 1 covers the basic background of fuel cell. The application of fuel cell technology in various fields, comparison of the different processes that leads to conversion of fuel to energy. It explains the hybridization of fuel cell technology in gas turbine cycle. The intermediate parts cover details of SOFC stack, types of stack design, their comparison in terms of application, hardware construction etc. It explains various components used in SOFC stack design, material used for their manufacturing. And the final part covers a basic understanding of reforming process and reactions involved in the reforming. Chapter 2 involves literature

review of the present work. The initial part of Chapter 3 helps in understanding the modelling techniques used. The following part explains the heat transfer modes modelled, the solver methodology used to solve energy and momentum equation. And the final part consists of property calculation of reacting mixtures, species transport model and the solver methodology to update species variations. Chapter 4 deals with discretizing and solving the governing energy equation of fluid flow and heat transfer for the entire stack model. Validation of the model and results for different simulation cases are studied in Chapter 5. Chapter 6 contains the conclusion drawn from the study and finally Chapter 7 gives future scope for development.

Chapter 2

LITERATURE REVIEW

SOFC has attracted considerable interest over last few decades due to its high efficiency and a friendly source of power generation. It has a potential to be used in various application right from stationery to transportation power generation systems. Direct or indirect source of Hydrogen like hydrocarbons can be directly used as a fuel thus making it compatible for various fuel sources. Integration of SOFC with Gas turbine or use of SOFC for small scale power generation like residential homes, military applications, auxiliary power unit for trucks has made SOFC a standalone technology for both large scale as well as distributed power generation systems. Due to this extensive applicability many researchers over the years have carried out a thorough study involving both theoretical as well experimental work. Theoretical as well as simulation of the various possible configuration of SOFC hybrid systems are put forward and the resources of these work are available in the open literature. Work presented in [7] considers the overall GT-cycle simulation where all the auxiliary components like the fuel cell, recuperator, combustor are considered as a lumped system, this helps in understanding the entire working of the cycle by reducing the complexities at the component level. While work carried out in [8] explains the details modeling at the component level to address the intricacy at the component level due various operating conditions of temperature, pressure, flow rate, heat generation etc. Work presented in [9] explains the effect of operating variable like pressure and fuel flow rate on the components and thus on system, increased pressure increases the system efficiency whereas increased flow rate decreases the efficiency. It also explains the advantage of reforming in SOFC hybrid system thus presenting results of electrical efficiency of 60 percent and system efficiency of 80 percent using internal reforming. Further the work carried out in [10] studies the effect of fuel

utilization rate on planar SOFC model in terms of temperature and I-V characteristics, it explains the effect of polarization, activation and diffusion limitations at electrode at high fuel utilization. The transient characteristics of fuel cell gas turbine hybrid system, its dynamics and performance are explained in [12]. In this study transient performance of a 60 kW Capstone recuperated gas turbine was compared against an SOFC integrated 60 KW capstone gas turbine and results proved that if all the operating conditions are stringently maintained the hybrid system has a quick thermal response compared to ordinary system. Similar work has been done in [13] by studying dynamic behavior of tubular SOFC using the control volume numerical simulation technique. The collective effect of heat transfer, electrochemical and species transport are accounted to study the dynamic behavior. Both steady and unsteady analysis is carried out to analyze the behavior of state variable, current and potential distribution. Further, research carried in [14] explains the significance of the stack design on the overall system performance, it involves the study of different stack configuration and proves that the counter-flow arrangement of the planar SOFC has least thermal gradients compared to the parallel flow and the cross flow under similar operating parameters and boundary conditions. A numerical simulation for flow and electrochemical behavior was studied to predict flow, temperature, current density, and fuel utilization for different stack design. [15] carries out a detail numerical analysis of a tubular SOFC, to simulate heat and species transport process, it explains the applicability of using a complete field solution for the heat and mass transfer instead of using the laminar flow assumptions which deviates from actual behavior significantly. Different models explaining the process of reforming are explained in [3]. Cell to cell voltage variation is studied in [16], it explains the influence of radiation, non-uniform flow rate, heat flux and other factor that cause voltage difference in the adjacent cell thus affecting the overall cell voltage. Work

presented in [5] provides a large data for thermodynamics property variation as a function of temperature for SOFC modeling.

Chapter 3

MODELING

3.1 Modeling Methodology

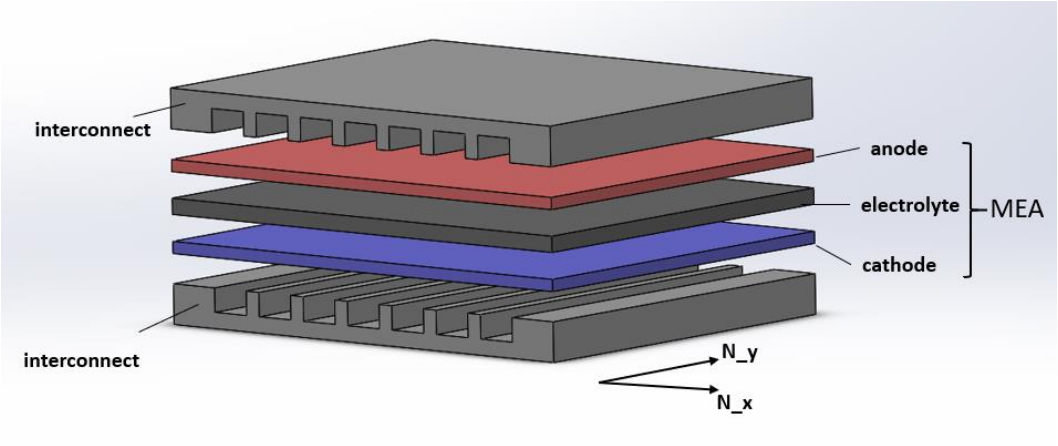

Figure 3-1 Stack model used for analysis

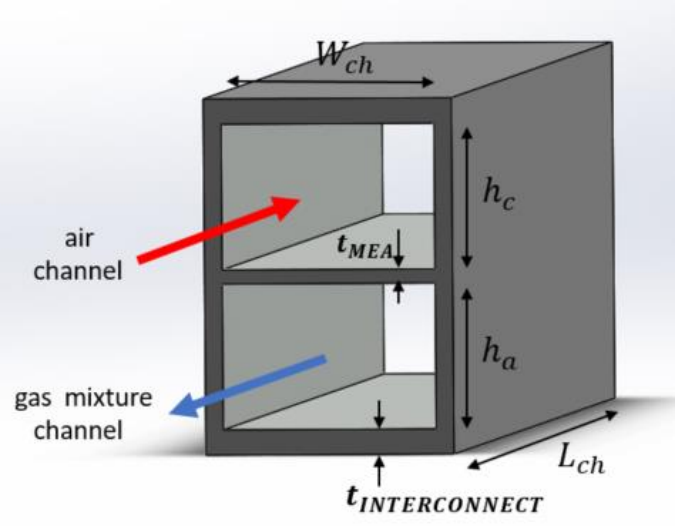

Figure 3-2 Unit model used for analysis

The finite volume discretization technique is used to discretize the entire domain to model the process of heat transfer and fluid flow through the stack [20]. The domain is divided in N_y number of control volumes along the flow direction. N_x represents the number of channel through which the fluid enters and leaves. The convection-diffusion form of energy equation is used to model the fluid flow through the anode and the cathode channel. The conduction form of energy equation is used to model conductive heat transfer through the ribs, interconnect and the membrane electrode assembly (MEA) (anode, cathode, electrolyte together is called as MEA). Thermodynamic species balance and chemical kinetics to model chemical mixture. Due to the repeated nature of the geometry, only a single unit consisting of anode channel, cathode channel, MEA and interconnect is simulated. As represented by the Figure 3-2 a single cell showing various dimension is modelled. The advantage of modeling a single cell is ease in analysis and saving considerable simulation time.

The following are the two modes of heat transfer considered,

Primary mode of heat transfer

Convective heat transfer from hot air at cathode to the MEA and interconnect and from MEA and interconnect to the gaseous mixture at the anode.

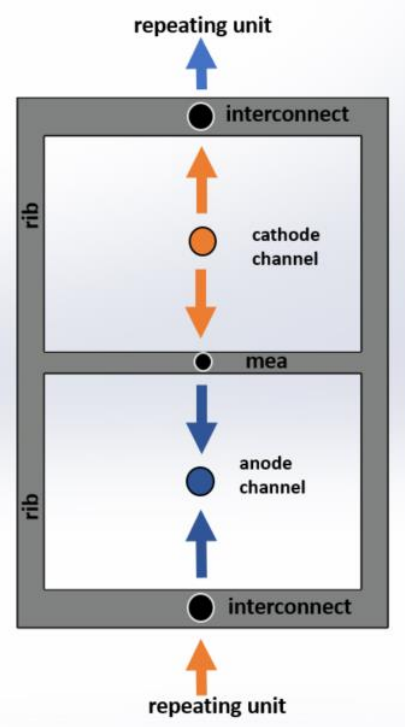

Figure 3-3 Representation of primary mode of heat transfer

Secondary mode of heat transfer

Convective heat transfer from hot air to ribs at cathode, conductive heat transfer through ribs to nodal plate at MEA and to interconnect. Conductive heat transfer from nodal plate at MEA and interconnect to ribs at anode, and finally convective heat transfer from ribs to gaseous mixture at the anode.

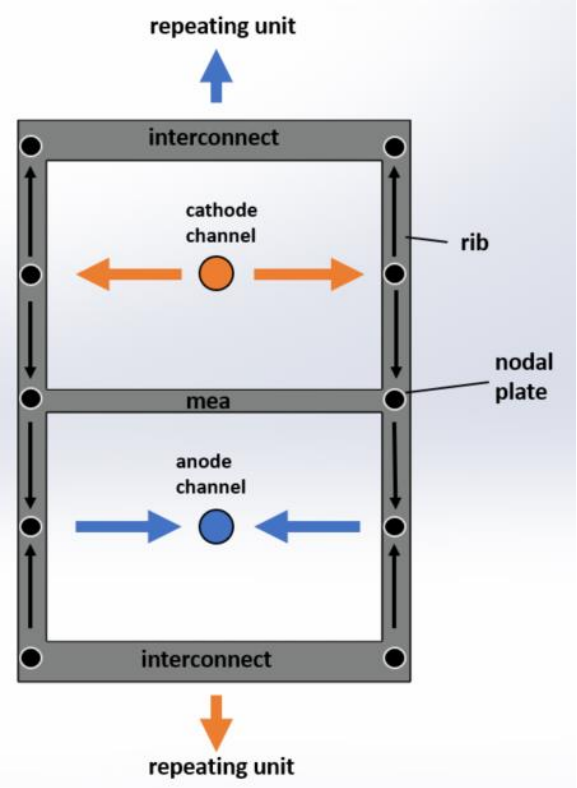

Figure 3-4 Representation of secondary mode of heat transfer

3.2 Working of the Solver

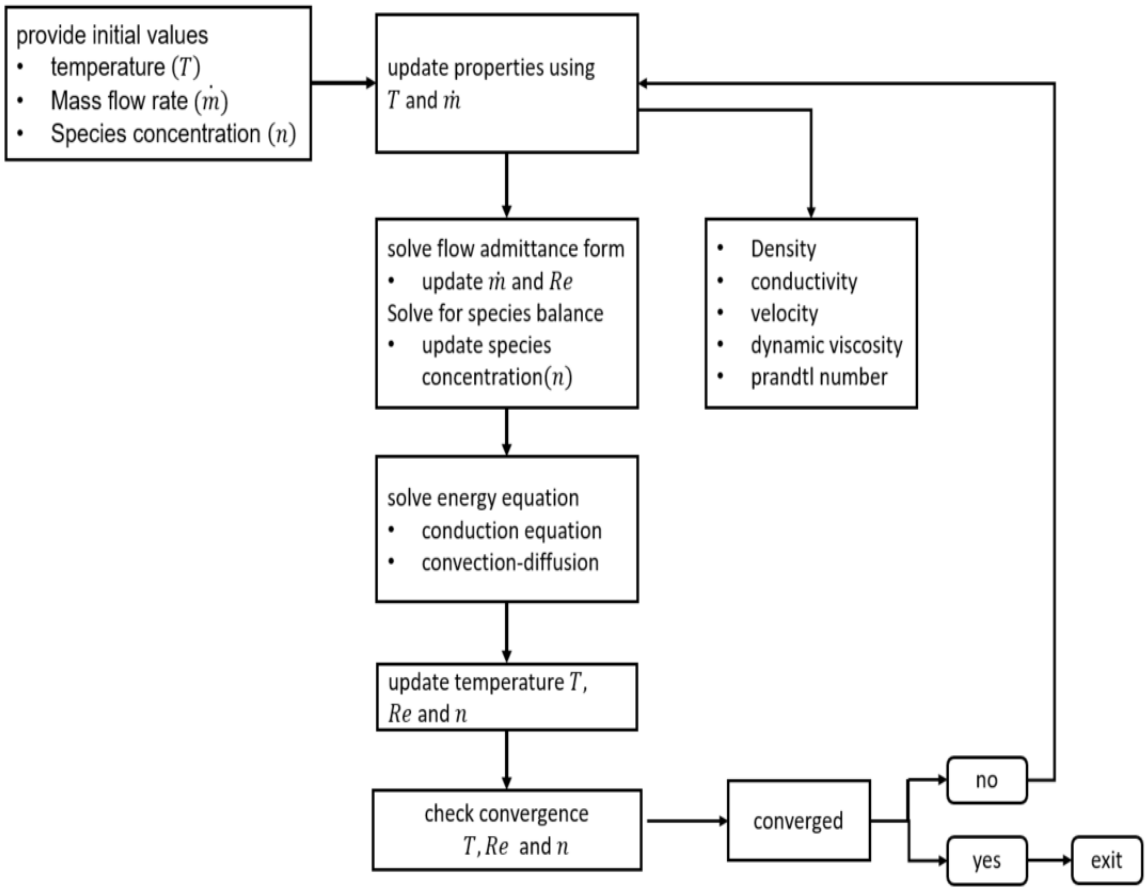

Figure 3-5 Working of the solver

3.3 Working of momentum module

The working of a 1-D momentum equation for a flow through a channel assuming negligible property variation and linear pressure drop along the flow is represented in the Figure 3-6. It is important to note that all the properties like velocity, mass flow rate, density etc. in the figure are averaged values over a channel.

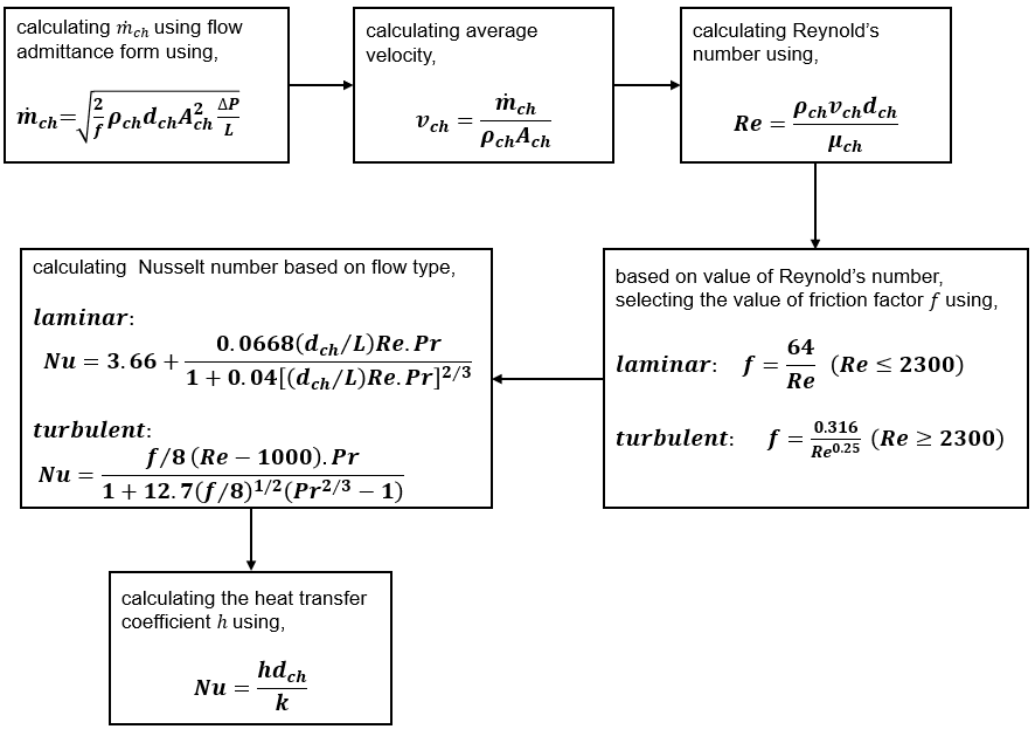

Figure 3-6 Working of the momentum module [18]

3.4 Property calculations

3.4.1 Viscosity model

To calculate the viscosity of gas mixture, the following semi-empirical formula derived for multicomponent mixture by Chapman-Enskog is used [6],

$$\mu_{mix}=\sum_{\alpha=1}^{N}\frac{x_\alpha\mu_\alpha}{\sum_\beta x_\beta \emptyset_{\alpha\beta}}$$

Where $\emptyset_{\alpha\beta}$ is a dimensionless quantity,

Where,

$$\emptyset_{\alpha\beta} = \frac{1}{\sqrt{8}}\left(1+\frac{M_\alpha}{M_\beta}\right)^{-0.5}\left[1+\left(\frac{\mu_\alpha}{\mu_\beta}\right)^{0.5}\left(\frac{M_\alpha}{M_\beta}\right)^{0.25}\right]^2$$

N represents the total number of species in the mixture.

χ_α is the mole fraction of an individual component α .

μ_α is the viscosity of an individual component α .

M_α is the molecular weight of an individual component α .

The regression values mentioned in the table are the viscosity of an individual component.

Table 3.4.1 Dynamic viscosity μ of the species (valid for 273-1473 K) [5]

Species	*C0*	*C1*	*C2*	*C3*	*C4*	*C5*	*C6*
CH_4	*-9.9989*	*529.37*	*-543.82*	*548.11*	*-367.06*	*140.48*	*-22.920*
H_2O	*-6.7541*	*244.93*	*419.50*	*-522.38*	*348.12*	*-126.96*	*19.591*
H_2	*15.553*	*299.78*	*-244.34*	*249.41*	*-167.51*	*62.966*	*-9.9892*
CO	*-4.9137*	*793.65*	*875.90*	*883.75*	*-572.14*	*208.42*	*-32.298*
CO_2	*-20.434*	*680.07*	*-432.49*	*244.22*	*-85.929*	*14.450*	*-0.4564*
O_2	*-1.6918*	*889.75*	*-892.79*	*905.98*	*-598.36*	*221.64*	*-34.754*
N_2	*1.2719*	*771.45*	*-809.20*	*832.47*	*-553.93*	*206.15*	*-32.430*

3.4.2 Thermal Conductivity model

Similar, to the viscosity model, semi-empirical formula derived for thermal conductivity of multicomponent mixture by Chapman-Enskog is [6],

$$k_{mix} = \sum_{\alpha=1}^{N} \frac{x_\alpha k_\alpha}{\sum_\beta x_\beta \emptyset_{\alpha\beta}}$$

Where $\emptyset_{\alpha\beta}$ is a dimensionless quantity,

$$\emptyset_{\alpha\beta} = \frac{1}{\sqrt{8}}\left(1+\frac{M_\alpha}{M_\beta}\right)^{-0.5}\left[1+\left(\frac{k_\alpha}{k_\beta}\right)^{0.5}\left(\frac{M_\alpha}{M_\beta}\right)^{0.25}\right]^2$$

Where,

N represents the total number of species in the mixture.

χ_α is the mole fraction of an individual component α .

M_α is the molecular weight of an individual component α .

k_α is the thermal conductivity of an individual component α .

The regression values mentioned in the table are the thermal conductivity of an individual component.

Table 3.4.2 Thermal conductivity K of the species (valid for 273-1473 K) [5]

Species	*C0*	*C1*	*C2*	*C3*	*C4*	*C5*	*C6*
CH_4	*0.4796*	*1.8732*	*37.413*	*-47.440*	*38.251*	*-17.283*	*3.2774*
H_2O	*2.0103*	*-7.9139*	*35.922*	*-41.390*	*35.993*	*-18.974*	*4.1531*
H_2	*1.5040*	*62.892*	*-47.763*	*47.763*	*-31.939*	*11.972*	*-1.8954*
CO	*-0.2815*	*13.999*	*-23.186*	*36.018*	*-30.818*	*13.379*	*-2.3224*
CO_2	*2.8888*	*-27.018*	*129.65*	*-233.29*	*216.83*	*-101.12*	*18.698*
O_2	*-0.1857*	*11.118*	*-7.3734*	*6.7130*	*-4.1797*	*1.4910*	*-0.2278*
N_2	*-0.3216*	*14.810*	*-25.473*	*38.837*	*-32.133*	*13.493*	*-2.2741*

3.4.3 Specific heat model

As the operating temperature inside the stack is very high it can be assumed that mixture behaves like ideal gas mixture. And at high temperature the specific heat is a function of temperature [5].

$$C_p = \sum_{i=0}^{6} \alpha_i \tau^i \quad where\ \tau = \frac{T(K)}{1000}$$

Future, the molar heat capacity of the ideal gas mixture consisting of N species can be

calculated as follows,

$$C_p(T) = \sum_{i=1}^{N} x_i C_{p_i}(T)$$

where x_i represents mole fraction of the $i\text{th}$ component.

The regression values mentioned in the table are the specific heat of the individual component.

Table 3.4.3 Specific heat of the species (valid for 273-1473K) [5]

Species	*C0*	*C1*	*C2*	*C3*	*C4*	*C5*	*C6*
CH_4	*47.964*	*-178.59*	*712.55*	*-1068.7*	*856.93*	*-358.75*	*61.321*
H_2O	*37.373*	*-41.205*	*146.01*	*-217.08*	*181.54*	*-79.409*	*14.015*
H_2	*21.157*	*56.036*	*-150.55*	*199.29*	*-136.15*	*46.903*	*-6.4725*
CO	*30.429*	*-8.1781*	*5.2062*	*41.974*	*-66.346*	*37.756*	*-7.6538*
CO_2	*4.3669*	*204.60*	*-471.33*	*657.88*	*-519.9*	*241.58*	*35.992*
O_2	*34.850*	*-57.975*	*203.68*	*-300.37*	*231.72*	*-91.821*	*14.776*
N_2	*29.027*	*4.8987*	*-38.040*	*105.17*	*-113.56*	*55.554*	*-10.350*

3.5 Species Transport

The generalized thermodynamic species balance for the chemical species undergoing SR and WGS reactions is of the form,

$$n|_{in} + \alpha(n|_{SR}) + \beta(n|_{WGS}) - n|_{out} = 0$$

Where,

α and β are the stoichiometric coefficients for the species.

$n|_{in}$ and $n|_{out}$ are the moles of a species (mol/s) entering and leaving a C.V.

Therefore, moles of different species can be calculated as follows,

$$CH_4 : n_{CH_4}|_{out} = n_{CH_4}|_{in} - \left(n_{CH_4}|_{SR}\right)$$

$$H_2O : n_{H_2O}|_{out} = n_{H_2O}|_{in} - \left(n_{CH_4}|_{SR}\right) - (n_{CO}|_{WGS})$$

$$H_2 : n_{H_2}|_{out} = n_{H_2}|_{in} + 3\left(n_{CH_4}|_{SR}\right) + (n_{CO}|_{WGS})$$

$$CO : n_{CO}|_{out} = n_{CO}|_{in} + (n_{CO}|_{SR}) - (n_{CO}|_{WGS})$$

$$CO_2 : n_{CO_2}|_{out} = n_{CO_2}|_{in} + (n_{CO}|_{WGS})$$

The conversion of CH_4 to H_2 by reforming reaction is described by forward reaction rate as,

$$n_{CH_4}|_{SR} = k_{SR}\left[\alpha_{CH_4}\alpha_{H_2o} - \frac{\alpha_{co}\alpha_{H_2}^3}{K_{p\_SR}}\right]$$

Similarly, the conversion rate CO to H_2 is described by the shifting reaction as,

$$n_{CO}|_{WGS} = k_{WGS}\left[\alpha_{CO}\alpha_{H_2o} - \frac{\alpha_{CO_2}\alpha_{H_2}}{K_{p\_WGS}}\right]$$

Where, α represent activity of the respective species which is calculated as,

$$\alpha = \frac{y\,P_{total}}{P_{atm}}$$

y is the mole fraction of respective components.

$k_{SR} = k_{WGS} = k_{reaction}$, represent reaction rate expressed in moles per second.

$$k_{reaction} = A_{reaction}exp\left(\frac{-E_{a\_rxn}}{RT}\right)$$

The numerical values of the pre-exponential factor used are [1],

$$A_{CH_4\_SR} = 4.225 \times 10^{15}\ mol/s\ \ for\ SR\ reaction$$

$$A_{co\_WGS} = 1.955 \times 10^{6}\ mol/s\ \ for\ WGS\ reaction$$

The values of activation energy are,

$$E_{a\_SR} = 240010\ J/mol\ \ for\ SR\ reaction$$

$$E_{a\_WGS} = 67130\ J/mol\ \ for\ WGS\ reaction$$

The equilibrium constant is calculated using,

$$K_{p\_SR} = exp\left(\frac{-\Delta G_{SR}}{RT}\right)$$

$$K_{p\_WGS} = exp\left(\frac{-\Delta G_{WGS}}{RT}\right)$$

ΔG, represents Gibbs free energy.

T in all the above formulae represent the fin or rib temperature.

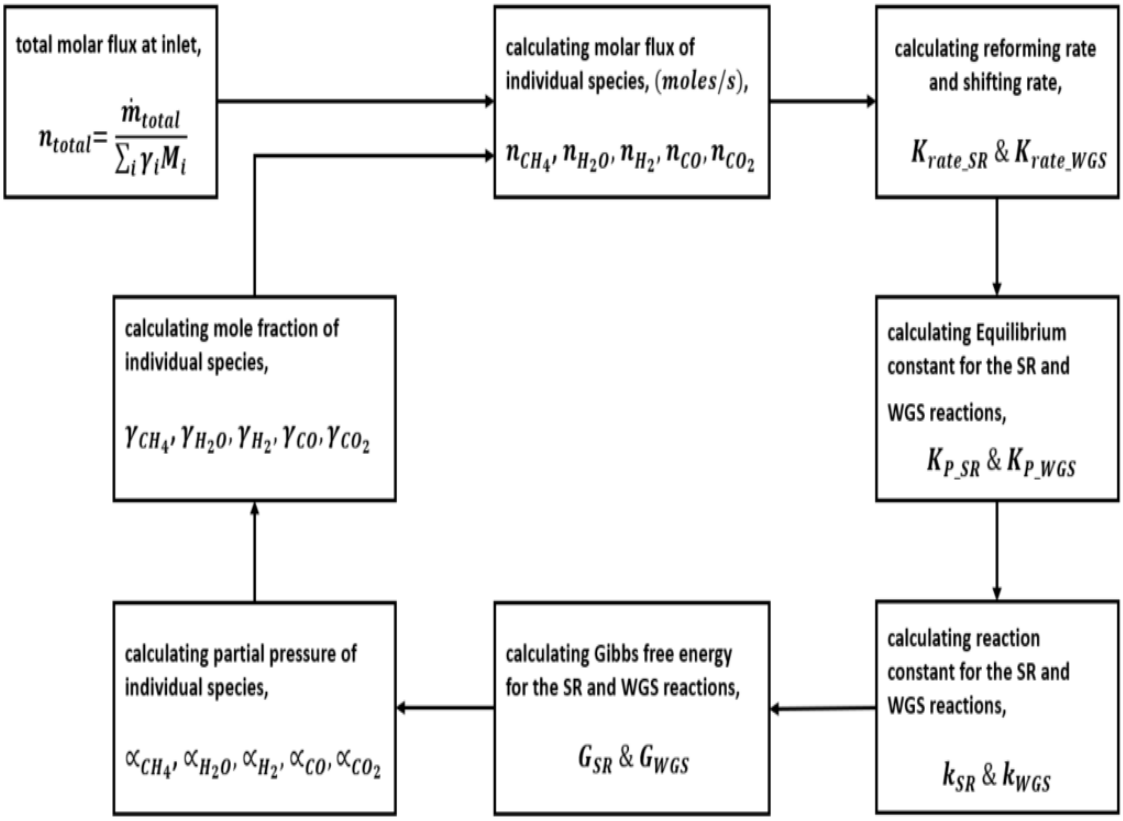

Figure 3-7 Working of the species transport module

Chapter 4

DISCRETIZATION OF THE MODEL

4.1 Discretization of fluid channel

Solving the 1-D steady state convection-diffusion form of energy equation,

$$\rho c_p u \frac{\partial T}{\partial y} = \frac{\partial}{\partial y}\left(k \frac{\partial T}{\partial y}\right) + u \frac{\partial P}{\partial y} + \dot{q}_{to\_gas} \tag{1}$$

Where,

$$\dot{q}_{to\_gas} = \dot{q}_{conn\_gas} + \dot{q}_{MEA\_gas} + \dot{q}_{ribs\_gas} + \dot{q}_{SR\_\&\_WGS} \tag{2}$$

$\dot{q}_{to\_gas}$ is the volumetric heat generation rate.

$\dot{q}_{conn\_gas}$ is the convective heat transfer from interconnect to the gas channel.

$\dot{q}_{MEA\_gas}$ is the convective heat transfer from MEA to the gas channel.

$\dot{q}_{ribs\_gas}$ is the convective heat transfer from ribs to the gas channel.

$\dot{q}_{SR\_\&\_WGS}$ is enthalpy exchange due to SR and WGS reaction.

The LHS of equation (1) can be written as,

$$\rho c_p u \frac{\partial T}{\partial y} = \frac{\partial\left(\rho c_p u T\right)}{\partial y} - c_p T \frac{\partial(\rho u)}{\partial y} - \rho u T \frac{\partial c_p}{\partial y} \tag{3}$$

Substituting equation (3) in (1),

$$\frac{\partial\left(\rho c_p u T\right)}{\partial y} - c_p T \frac{\partial(\rho u)}{\partial y} - \rho u T \frac{\partial c_p}{\partial y} = \frac{\partial}{\partial y}\left(k \frac{\partial T}{\partial y}\right) + u \frac{\partial P}{\partial y} + \dot{q}_{to\_gas} \tag{4}$$

Rearranging the above equation (4),

$$\frac{\partial}{\partial y}\left(\rho c_p u T - k\frac{\partial T}{\partial y}\right) = c_p T\frac{\partial(\rho u)}{\partial y} + \rho u T\frac{\partial c_p}{\partial y} + u\frac{\partial P}{\partial y} + \dot{q}_{to\_gas} \tag{5}$$

Considering LHS of equation (5),

$$\frac{\partial}{\partial y}\left(\rho c_p u T - k\frac{\partial T}{\partial y}\right) = \frac{\partial}{\partial y}\left[c_p\left(\rho u T - \frac{k}{c_p}\frac{\partial T}{\partial y}\right)\right]$$

Further solving results in,

$$\frac{\partial}{\partial y}\left[c_p\left(\rho u T - \frac{k}{c_p}\frac{\partial T}{\partial y}\right)\right] = \frac{\partial c_p}{\partial y}\left(\rho u T - \frac{k}{c_p}\frac{\partial T}{\partial y}\right) + c_p\frac{\partial}{\partial y}\left(\rho u T - \frac{k}{c_p}\frac{\partial T}{\partial y}\right) \tag{6}$$

Substituting equation (6) in (5),

$$\frac{\partial c_p}{\partial y}\left(\rho u T - \frac{k}{c_p}\frac{\partial T}{\partial y}\right) + c_p\frac{\partial}{\partial y}\left(\rho u T - \frac{k}{c_p}\frac{\partial T}{\partial y}\right)$$

$$= c_p T\frac{\partial(\rho u)}{\partial y} + \rho u T\frac{\partial c_p}{\partial y} + u\frac{\partial P}{\partial y} + \dot{q}_{to\_gas} \tag{7}$$

Cancelling $\rho u T\frac{\partial c_p}{\partial y}$ from both sides and dividing c_p,

$$\frac{\partial}{\partial y}\left(\rho u T - \frac{k}{c_p}\frac{\partial T}{\partial y}\right) = T\frac{\partial(\rho u)}{\partial y} + \frac{u}{c_p}\frac{\partial P}{\partial y} + \frac{1}{c_p}\dot{q}_{to\_gas} + \frac{k}{c_p^2}\frac{\partial T}{\partial y}\frac{\partial c_p}{\partial y} \tag{8}$$

Which can be written as,

$$\frac{\partial}{\partial y}\left(\rho u\phi - \Gamma\frac{\partial \phi}{\partial y}\right) = \phi\frac{\partial(\rho u)}{\partial y} + S \tag{9}$$

where,

$\phi = T$

$\Gamma = \frac{k}{c_p}$

$$S = \frac{u}{c_p}\frac{\partial P}{\partial y} + \frac{1}{c_p}\dot{q}_{to\_gas} + \frac{k}{c_p^2}\frac{\partial T}{\partial y}\frac{\partial c_p}{\partial y}$$

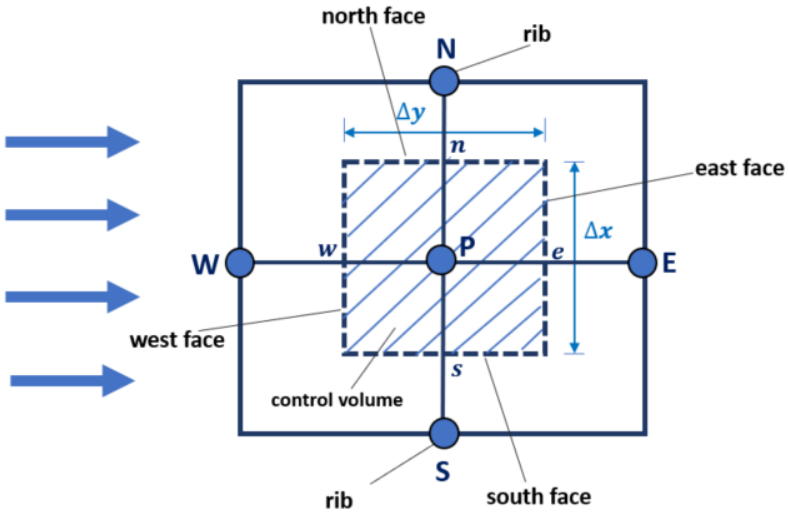

Figure 4-1 Finite volume grid for the flow channel in horizontal plane

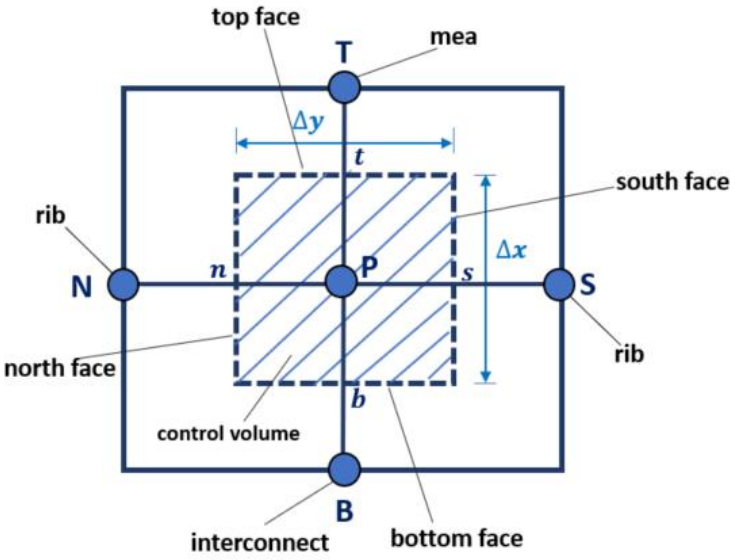

Figure 4-2 Finite volume grid for the flow channel in vertical plane

Integrating and applying Gauss Divergence Theorem to equation (9) results in,

$$\int \frac{\partial}{\partial y}\left(\rho u\phi - \Gamma\frac{\partial \phi}{\partial y}\right) dV = \int \phi \frac{\partial(\rho u)}{\partial y} dV + S\Delta y A_c \tag{10}$$

Considering LHS of equation (10),

$$\int \frac{\partial}{\partial y}\left(\rho u\phi - \Gamma\frac{\partial \phi}{\partial y}\right) dV = \int_w^e \frac{\partial}{\partial y}\left(\rho u\phi - \Gamma\frac{\partial \phi}{\partial y}\right) dA$$

$$= \left[\left(\rho u\phi - \Gamma\frac{\partial \phi}{\partial y}\right) A_c\right]_e - \left[\left(\rho u\phi - \Gamma\frac{\partial \phi}{\partial y}\right) A_c\right]_w$$

$$= \left[(\rho u\phi A_c)_e - \left(\Gamma\frac{\partial \phi}{\partial y} A_c\right)_e\right] - \left[(\rho u\phi A_c)_w - \left(\Gamma\frac{\partial \phi}{\partial y} A_c\right)_w\right] \tag{11}$$

Considering first term in the RHS of equation (10),

$$\int \phi \frac{\partial(\rho u)}{\partial y} dV = \phi_p \int_w^e \rho u dA = \phi_p [\rho u A_c]_w^e$$

$$= \phi_p [\rho u A_c]_e - \phi_p [\rho u A_c]_w \tag{12}$$

Substituting equations (11) and (12) in (10),

$$\left[(\rho u \phi A_c)_e - \left(\Gamma \frac{\partial \phi}{\partial y} A_c\right)_e\right] - \left[(\rho u \phi A_c)_w - \left(\Gamma \frac{\partial \phi}{\partial y} A_c\right)_w\right] =$$

$$\phi_P [\rho u A_c]_e - \phi_P [\rho u A_c]_w + S \Delta y A_c \tag{13}$$

Now the value of ϕ on the west and the east face is approximated as follows,

$$\phi_e = \frac{\phi_P + \phi_E}{2} \; and \; \phi_w = \frac{\phi_W + \phi_P}{2}$$

Also, the differential of ϕ on the west and the east face is approximated as follows,

$$\left(\frac{\partial \phi}{\partial y}\right)_e = \frac{\phi_E - \phi_P}{\Delta y} \; and \left(\frac{\partial \phi}{\partial y}\right)_w = \frac{\phi_P - \phi_W}{\Delta y}$$

Substituting the above values in equation (13),

$$(\rho u A_c)_e \frac{\phi_P + \phi_E}{2} - (\Gamma A_c)_e \frac{\phi_E - \phi_P}{\Delta y} - (\rho u A_c)_w \frac{\phi_W + \phi_P}{2}$$

$$+ (\Gamma A_c)_e \frac{\phi_P - \phi_W}{\Delta y} = \phi_P (\rho u A_c)_e - \phi_P (\rho u A_c)_w + S \Delta y A_c \tag{14}$$

Which can be simplified to,

$$\frac{(\rho u A_c)_e}{2} \phi_P + \frac{(\rho u A_c)_e}{2} \phi_E - \left(\frac{\Gamma A_c}{\Delta y}\right)_e \phi_E + \left(\frac{\Gamma A_c}{\Delta y}\right)_e \phi_P - \frac{(\rho u A_c)_w}{2} \phi_W$$

$$- \frac{(\rho u A_c)_w}{2} \phi_P + \left(\frac{\Gamma A_c}{\Delta y}\right)_w \phi_P - \left(\frac{\Gamma A_c}{\Delta y}\right)_e \phi_W = \phi_P (\rho u A_c)_e - \phi_P (\rho u A_c)_w$$

$$+S\Delta yA_c \tag{15}$$

Now the source term is,

$$S = \frac{u}{c_p}\frac{\partial P}{\partial y} + \frac{1}{c_p}\dot{q}_{to\_gas} + \frac{k}{c_p^2}\frac{\partial \phi}{\partial y}\frac{\partial c_p}{\partial y}$$

Of which $\dot{q}_{to\_gas}$ is modelled as,

$$\dot{q}_{to\_gas} = \frac{h_{fluid}A_{conv_{MEA}}(\phi_{MEA} - \phi_{fluid})}{\Delta yA_c} + \frac{h_{fluid}A_{conv_{conn}}(\phi_{conn} - \phi_{fluid})}{\Delta yA_c}$$

$$+ \frac{h_{fluid}A_{conv\_rib\_R}(\phi_{rib\_R} - \phi_{fluid})}{\Delta yA_c} + \frac{h_{fluid}A_{conv\_rib\_L}(\phi_{rib\_L} - \phi_{fluid})}{\Delta yA_c}$$

$$-\frac{\phi_{fluid}}{\Delta yA_c}\left(n_{CH_4}|_{SR}C_{p\_CH_4} + n_{H_2O}|_{SR}C_{p\_H_2O} + n_{CO}|_{WGS}C_{p\_Co} + n_{H_2O}|_{WGS}C_{p\_H_2O}\right)$$

$$+\frac{\phi_{rib\_L}}{\Delta yA_c}\left(n_{CO}|_{SR}C_{p\_CO} + 3\,n_{H_2}|_{SR}C_{p\_H_2} + n_{CO_2}|_{WGS}C_{p\_CO_2} + n_{H_2}|_{WGS}C_{p\_H_2}\right)$$

$$+\frac{\phi_{rib\_R}}{\Delta yA_c}\left(n_{CO}|_{SR}C_{p\_CO} + 3\,n_{H_2}|_{SR}C_{p\_H_2} + n_{CO_2}|_{WGS}C_{p\_CO_2} + n_{H_2}|_{WGS}C_{p\_H_2}\right) \tag{16}$$

Therefore, the source term now becomes,

$$S = \frac{u}{c_p}\frac{\partial P}{\partial y} + \frac{1}{c_p}\left(\frac{h_{fluid}A_{conv\_MEA}(\phi_{MEA} - \phi_{fluid})}{\Delta yA_c}\right.$$

$$+\frac{h_{fluid}A_{conv\_conn}(\phi_{conn} - \phi_{fluid})}{\Delta yA_c} + \frac{h_{fluid}A_{conv\_rib\_R}(\phi_{rib\_R} - \phi_{fluid})}{\Delta yA_c}$$

$$\left.+\frac{h_{fluid}A_{conv\_rib\_L}(\phi_{rib\_L} - \phi_{fluid})}{\Delta yA_c}\right)$$

$$-\frac{\phi_{fluid}}{c_p\Delta yA_c}\left(n_{CH_4}|_{SR}C_{p\_CH_4} + n_{H_2O}|_{SR}C_{p\_H_2O} + n_{CO}|_{WGS}C_{p\_Co} + n_{H_2O}|_{WGS}C_{p\_H_2O}\right)$$

$$+ \quad \frac{\phi_{rib\_L}}{c_p \Delta y A_c}\left(n_{CO}|_{SR} C_{p\_CO} + 3\, n_{H_2}\big|_{SR} C_{p\_H_2} + n_{CO_2}\big|_{WGS} C_{p\_CO_2} + n_{H_2}\big|_{WGS} C_{p\_H_2}\right)$$

$$+ \frac{\phi_{rib\_R}}{c_p \Delta y A_c}\left(n_{CO}|_{SR} C_{p\_CO} + 3\, n_{H_2}\big|_{SR} C_{p\_H_2} + n_{CO_2}\big|_{WGS} C_{p\_CO_2} + n_{H_2}\big|_{WGS} C_{p\_H_2}\right)$$

$$+ \frac{k}{c_p^2}\frac{\partial \phi}{\partial y}\frac{\partial c_p}{\partial y} \tag{17}$$

Now,

$$S \Delta y A_c = \frac{u}{c_p}\Delta P A_c + \left(\frac{h_{fluid} A_{conv\_MEA}\left(\phi_{MEA} - \phi_{fluid}\right)}{c_p}\right.$$

$$+ \frac{h_{fluid} A_{conv\_conn}\left(\phi_{conn} - \phi_{fluid}\right)}{c_p} + \frac{h_{fluid} A_{conv\_rib\_R}\left(\phi_{rib\_R} - \phi_{fluid}\right)}{c_p}$$

$$\left. + \frac{h_{fluid} A_{conv\_rib\_L}\left(\phi_{rib\_L} - \phi_{fluid}\right)}{c_p}\right)$$

$$- \frac{\phi_{fluid}}{c_p}\left(n_{CH_4}\big|_{SR} C_{p\_CH_4} + n_{H_2O}\big|_{SR} C_{p\_H_2O} + n_{CO}|_{WGS} C_{p\_Co} + n_{H_2O}\big|_{WGS} C_{p\_H_2O}\right)$$

$$+ \frac{\phi_{rib\_L}}{c_p}\left(n_{CO}|_{SR} C_{p\_CO} + 3\, n_{H_2}\big|_{SR} C_{p\_H_2} + n_{CO_2}\big|_{WGS} C_{p\_CO_2} + n_{H_2}\big|_{WGS} C_{p\_H_2}\right)$$

$$+ \frac{\phi_{rib\_R}}{c_p}\left(n_{CO}|_{SR} C_{p\_CO} + 3\, n_{H_2}\big|_{SR} C_{p\_H_2} + n_{CO_2}\big|_{WGS} C_{p\_CO_2} + n_{H_2}\big|_{WGS} C_{p\_H_2}\right)$$

$$+ \frac{k}{c_p^2}\frac{\partial \phi}{\partial y}\Delta c_p A_c \tag{18}$$

Substituting equation (18) into (15),

$$\frac{(\rho u A_c)_e}{2}\phi_P + \frac{(\rho u A_c)_e}{2}\phi_E - \left(\frac{\Gamma A_c}{\Delta y}\right)_e \phi_E + \left(\frac{\Gamma A_c}{\Delta y}\right)_e \phi_P - \frac{(\rho u A_c)_w}{2}\phi_W$$

$$-\frac{(\rho u A_c)_w}{2}\phi_P+\left(\frac{\Gamma A_c}{\Delta y}\right)_w\phi_P-\left(\frac{\Gamma A_c}{\Delta y}\right)_e\phi_W=\phi_P(\rho u A_c)_e-\phi_P(\rho u A_c)_w$$

$$+\frac{u}{c_p}\Delta P A_c+\left(\frac{h_{fluid}A_{conv\_MEA}(\phi_{MEA}-\phi_P)}{c_p}\right.$$

$$+\frac{h_{fluid}A_{conv\_conn}(\phi_{conn}-\phi_P)}{c_p}+\frac{h_{fluid}A_{conv\_rib\_R}(\phi_{rib\_R}-\phi_P)}{c_p}$$

$$\left.+\frac{h_{fluid}A_{conv\_rib\_L}(\phi_{rib\_L}-\phi_P)}{c_p}\right)$$

$$-\frac{\phi_P}{c_p}\left(n_{CH_4}|_{SR}C_{p\_CH_4}+n_{H_2O}|_{SR}C_{p\_H_2O}+n_{CO}|_{WGS}C_{p\_Co}+n_{H_2O}|_{WGS}C_{p\_H_2O}\right)$$

$$+\frac{\phi_{rib\_L}}{c_p}\left(n_{CO}|_{SR}C_{p\_CO}+3\,n_{H_2}|_{SR}C_{p\_H_2}+n_{CO_2}|_{WGS}C_{p\_CO_2}+n_{H_2}|_{WGS}C_{p\_H_2}\right)$$

$$+\frac{\phi_{rib\_R}}{c_p}\left(n_{CO}|_{SR}C_{p\_CO}+3\,n_{H_2}|_{SR}C_{p\_H_2}+n_{CO_2}|_{WGS}C_{p\_CO_2}+n_{H_2}|_{WGS}C_{p\_H_2}\right)$$

$$+\frac{k}{c_p^2}\frac{\partial\phi}{\partial y}\Delta c_p A_c \qquad (19)$$

Now we define,

Convection factor for both east and west face as,

$$F_w=(\rho u)_w A_c \quad and \quad F_e=(\rho u)_e A_c$$

And diffusion factor as,

$$D_w=\left(\frac{\Gamma}{\Delta y}\right)_w A_c \;\; and \;\; D_e=\left(\frac{\Gamma}{\Delta y}\right)_e A_c$$

Substituting the above values in equation (19),

$$\frac{F_e}{2}\phi_P+\frac{F_e}{2}\phi_E-D_e\phi_E+D_e\phi_P-\frac{F_e}{2}\phi_W-\frac{F_w}{2}\phi_P+D_w\phi_P-D_w\phi_W$$

$$= \phi_P F_e - \phi_P F_w$$

$$+ \frac{u}{c_p} \Delta P A_c + \left(\frac{h_{fluid} A_{conv\_MEA} (\phi_{MEA} - \phi_P)}{c_p} \right.$$

$$+ \frac{h_{fluid} A_{conv\_conn} (\phi_{conn} - \phi_P)}{c_p} + \frac{h_{fluid} A_{conv\_rib\_R} (\phi_{rib\_R} - \phi_P)}{c_p}$$

$$\left. + \frac{h_{fluid} A_{conv\_rib\_L} (\phi_{rib\_L} - \phi_P)}{c_p} \right)$$

$$- \frac{\phi_P}{c_p} \left(n_{CH_4}|_{SR} C_{p\_CH_4} + n_{H_2O}|_{SR} C_{p\_H_2O} + n_{CO}|_{WGS} C_{p\_Co} + n_{H_2O}|_{WGS} C_{p\_H_2O} \right)$$

$$+ \frac{\phi_{rib\_L}}{c_p} \left(n_{CO}|_{SR} C_{p\_CO} + 3\, n_{H_2}|_{SR} C_{p\_H_2} + n_{CO_2}|_{WGS} C_{p\_CO_2} + n_{H_2}|_{WGS} C_{p\_H_2} \right)$$

$$+ \frac{\phi_{rib\_R}}{c_p} \left(n_{CO}|_{SR} C_{p\_CO} + 3\, n_{H_2}|_{SR} C_{p\_H_2} + n_{CO_2}|_{WGS} C_{p\_CO_2} + n_{H_2}|_{WGS} C_{p\_H_2} \right)$$

$$+ \frac{k}{c_p^2} \frac{\partial \phi}{\partial y} \Delta c_p A_c \qquad (20)$$

Rearranging the terms yields,

$$\left[-\frac{F_e}{2} + D_e + \frac{F_w}{2} + D_w + \frac{h_{fluid} A_{conv\_MEA}}{c_p} + \frac{h_{fluid} A_{conv\_conn}}{c_p} \right.$$

$$+ \frac{h_{fluid} A_{conv\_rib\_L}}{c_p} + \frac{h_{fluid} A_{conv\_rib\_R}}{c_p}$$

$$\left. + \frac{1}{c_p} \left(n_{CH_4}|_{SR} C_{p\_CH_4} + n_{H_2O}|_{SR} C_{p\_H_2O} + n_{CO}|_{WGS} C_{p\_Co} + n_{H_2O}|_{WGS} C_{p\_H_2O} \right) \right] \phi_P$$

$$= \left[-\frac{F_e}{2} + D_e \right] \phi_E + \left[\frac{F_w}{2} + D_w \right] \phi_W$$

$$+\frac{h_{fluid}A_{conv\_MEA}}{c_p}\phi_{MEA}+\frac{h_{fluid}A_{conv\_conn}}{c_p}\phi_{conn}$$

$$+\left(\frac{h_{fluid}A_{conv\_rib\_L}}{c_p}+\frac{1}{c_p}\left(n_{CO}|_{SR}C_{p\_CO}+3\,n_{H_2}\big|_{SR}C_{p\_H_2}+n_{CO_2}\big|_{WGS}C_{p\_CO_2}\right.\right.$$

$$\left.\left.+\,n_{H_2}\big|_{WGS}C_{p\_H_2}\right)\right)\phi_{rib\_L}$$

$$+\left(\frac{h_{fluid}A_{conv\_rib\_R}}{c_p}+\frac{1}{c_p}\left(n_{CO}|_{SR}C_{p\_CO}+3\,n_{H_2}\big|_{SR}C_{p\_H_2}+n_{CO_2}\big|_{WGS}C_{p\_CO_2}\right.\right.$$

$$\left.\left.+n_{H_2}\big|_{WGS}C_{p\_H_2}\right)\right)\phi_{rib\_R}$$

$$+\frac{u}{c_p}\Delta PA_c+\frac{k}{c_p^2}\frac{\partial\phi}{\partial y}\Delta c_pA_c \tag{21}$$

Therefore, we get

$$a_P\phi_P=a_E\phi_E+a_W\phi_W+a_{MEA}\phi_{MEA}+a_{conn}\phi_{conn}+a_{rib\_R}\phi_{rib\_R}$$
$$+\,a_{rib\_L}\phi_{rib\_L}+b \tag{22}$$

Table 4.1 Coefficients for Fluid channel

a_P	$-\frac{F_e}{2}+D_e+\frac{F_w}{2}+D_w+\frac{h_{fluid}A_{conv\_MEA}}{c_p}+\frac{h_{fluid}A_{conv\_conn}}{c_p}$ $+\frac{h_{fluid}A_{conv_{rib\_L}}}{c_p}+\frac{h_{fluid}A_{conv_{rib\_R}}}{c_p}$ $+\frac{1}{c_p}\left(n_{CH_4}\big\|_{SR}C_{p_{\_CH_4}}+n_{H_2O}\big\|_{SR}C_{p_{\_H_2O}}+n_{CO}\|_{WGS}C_{p\_Co}\right.$ $\left.+n_{H_2O}\big\|_{WGS}C_{p_{\_H_2O}}\right)$

a_E	$-\frac{F_e}{2} + D_e$
a_W	$\frac{F_w}{2} + D_w$
a_{MEA}	$\frac{h_{fluid} A_{conv\_MEA}}{c_p}$
a_{conn}	$\frac{h_{fluid} A_{conv\_conn}}{c_p}$
a_{rib_R}	$\frac{h_{fluid} A_{conv\_rib\_L}}{c_p} + \frac{1}{c_p}\left(n_{CO}\vert_{SR} C_{p\_CO} + 3\, n_{H_2}\vert_{SR} C_{p\_H_2} + n_{CO_2}\vert_{WGS} C_{p\_CO_2} + n_{H_2}\vert_{WGS} C_{p\_H_2}\right)$
a_{rib_L}	$\frac{h_{fluid} A_{conv\_rib\_R}}{c_p} + \frac{1}{c_p}\left(n_{CO}\vert_{SR} C_{p\_CO} + 3\, n_{H_2}\vert_{SR} C_{p\_H_2} + n_{CO_2}\vert_{WGS} C_{p\_CO_2} + n_{H_2}\vert_{WGS} C_{p\_H_2}\right)$
b	$\frac{u}{c_p}\Delta P A_c + \frac{k}{c_p^2}\frac{\partial \phi}{\partial y}\Delta c_p A_c$
a_P	$a_E + a_W + a_{MEA} + a_{conn} + a_{rib\_R} + a_{rib\_L}$

$a_W = D_W(1 - 0.5Pe_w)$

$a_E = D_E(1 - 0.5Pe_e)$

Using power law scheme the value at west and east face are,

$a_W = D_W[\![0, (1 - 0.1|Pe|^5)]\!] + [\![F_W, 0]\!]$

$$a_E = D_W[\![0, (1 - 0.1|Pe|^5)]\!] + [\![F_E, 0]\!]$$

According to above, if Pe is greater than 10, diffusion will be ignored. Using these coefficient, we solve iteratively for ϕ_P .

4.2. Discretization of Membrane Electrode Assembly (MEA)

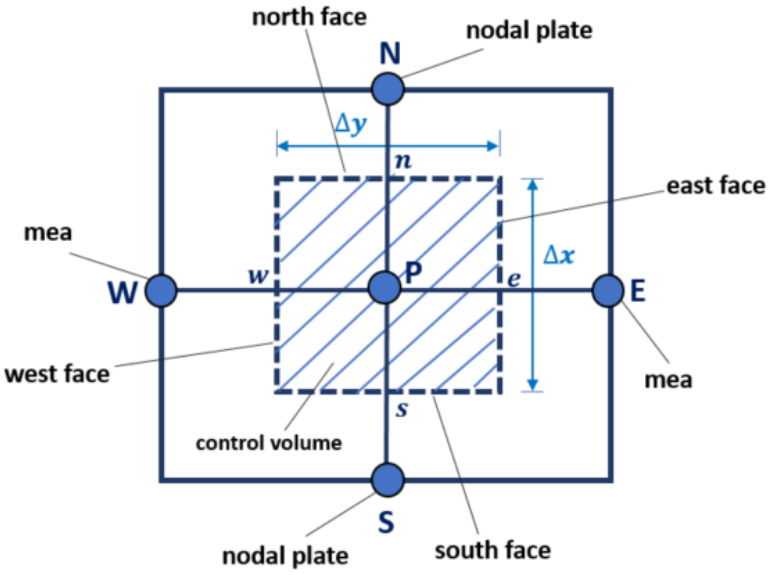

Figure 4-3 Finite volume grid for Membrane Electrode Assembly (MEA)

Consider 2-dimensional heat conduction equation

$$\rho c \frac{\partial T}{\partial t} = \frac{\partial}{\partial x}\left(k \frac{\partial T}{\partial x}\right) + \frac{\partial}{\partial y}\left(k \frac{\partial T}{\partial y}\right) + S \tag{23}$$

The steady state form of the above equation is

$$\frac{\partial}{\partial x}\left(k \frac{\partial T}{\partial x}\right) + \frac{\partial}{\partial y}\left(k \frac{\partial T}{\partial y}\right) + S = 0 \tag{24}$$

The source term *S* in the above equation represents the volumetric heat generation which is equal to $\ddot{s}_{MEA}$,

$$\frac{\partial}{\partial x}\left(k \frac{\partial T}{\partial x}\right) + \frac{\partial}{\partial y}\left(k \frac{\partial T}{\partial y}\right) + \ddot{s}_{MEA} = 0 \tag{25}$$

Integrating above equation over the control volume,

$$\int_V \frac{\partial}{\partial x}\left(k\frac{\partial T}{\partial x}\right)dV + \int_V \frac{\partial}{\partial y}\left(k\frac{\partial T}{\partial y}\right)dV + \int_V SdV = 0 \tag{26}$$

Applying the Gauss Divergence Theorem,

$$\int_A \left(k\frac{\partial T}{\partial x}\right)dA + \int_V \left(k\frac{\partial T}{\partial y}\right)dA + \int_V SdV = 0 \tag{27}$$

Where,

$$\int_V SdV = \dot{s}\Delta V = \dot{s}_{MEA}\Delta V \quad and \;\; \Delta V = dxdy.thk_{MEA} \tag{28}$$

The source term can be model as below,

$$\dot{s}_{MEA} = h_{hf}A_{conv\_MEA}(T_{hf} - T_{MEA}) - h_{hf}A_{conv\_MEA}(T_{MEA} - T_{cf}) \tag{29}$$

Substituting equation (28), (29) in (27)

$$\int_s^n \left(k\frac{\partial T}{\partial x}\right)dA + \int_w^e \left(k\frac{\partial T}{\partial y}\right)dA + h_{hf}A_{conv\_MEA}(T_{hf} - T_{MEA})$$

$$-h_{cf}A_{conv_{MEA}}(T_{MEA} - T_{cf}) = 0 \tag{30}$$

Which can be written as,

$$\left[kA_{c/s}\frac{\partial T}{\partial x}\right]_n - \left[kA_{c/s}\frac{\partial T}{\partial x}\right]_s + \left[kA_{c/s}\frac{\partial T}{\partial y}\right]_e - \left[kA_{c/s}\frac{\partial T}{\partial y}\right]_w$$

$$+ \left[h_{hf}A_{conv\_MEA}(T_{hf} - T_{MEA}) - h_{cf}A_{conv\_MEA}(T_{MEA} - T_{cf})\right] = 0 \tag{31}$$

Which can be further written as,

$$k_n A_{c/s\_n}\frac{T_N - T_P}{\Delta x} - k_s A_{c/s}\frac{T_P - T_S}{\Delta x} + k_e A_{c/s}\frac{T_E - T_P}{\Delta y} - k_w A_{c/s\_w}\frac{T_P - T_W}{\Delta y}$$

$$+ \left[h_{hf}A_{conv_{MEA}}(T_{hf} - T_P) - h_{cf}A_{conv_{MEA}}(T_P - T_{cf})\right] = 0$$

(32)

Which can be rearranged as,

$$\left[\frac{k_n A_{c/s\_n}}{\Delta x} + \frac{k_s A_{c/s\_s}}{\Delta x} + \frac{k_e A_{c/s\_e}}{\Delta y} + \frac{k_w A_{c/s\_w}}{\Delta y} + h_{hf} A_{conv\_MEA} + h_{cf} A_{conv\_MEA}\right] T_p$$

$$= \frac{k_n A_{c/s\_n}}{\Delta x} T_N + \frac{k_s A_{c/s\_s}}{\Delta x} T_S + \frac{k_e A_{c/s\_e}}{\Delta y} T_E + \frac{k_w A_{c/s\_w}}{\Delta y} T_W + h_{hf} A_{conv_{MEA}} T_{hf} + h_{cf} A_{conv_{MEA}} T_{cf} \quad (33)$$

Therefore, the discretized equation can be written as,

$$a_P T_P = a_N T_N + a_S T_S + a_E T_E + a_W T_W + b_{hf} T_{hf} + b_{cf} T_{cf} \quad (34)$$

Table 4.2 Coefficients for MEA

a_N	$\frac{k_n A_{c/s\_n}}{\Delta x}$
a_S	$\frac{k_s A_{c/s\_s}}{\Delta x}$
a_E	$\frac{k_e A_{c/s\_e}}{\Delta y}$
a_W	$\frac{k_w A_{c/s\_w}}{\Delta y}$
b_{hf}	$h_{hf} A_{conv_{MEA}}$
b_{cf}	$h_{cf} A_{conv_{MEA}}$

a_P	$a_N + a_S + a_E + a_W + b_{hf} + b_{cf}$

4.3. Discretization of Interconnect

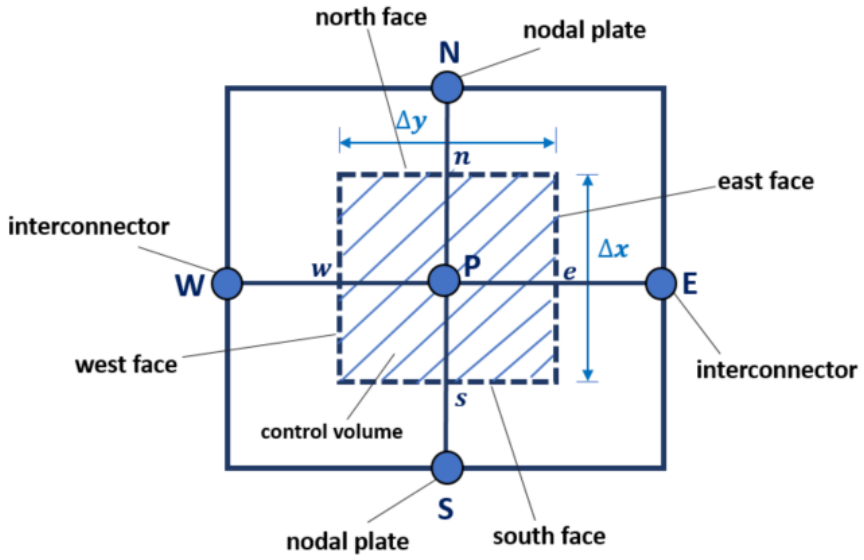

Figure 4-4 Finite volume grid for Interconnect

Consider 2-dimensional heat conduction equation

$$\rho c \frac{\partial T}{\partial t} = \frac{\partial}{\partial x}\left(k \frac{\partial T}{\partial x}\right) + \frac{\partial}{\partial y}\left(k \frac{\partial T}{\partial y}\right) + S \tag{35}$$

The steady state form of the above equation is

$$\frac{\partial}{\partial x}\left(k \frac{\partial T}{\partial x}\right) + \frac{\partial}{\partial y}\left(k \frac{\partial T}{\partial y}\right) + S = 0 \tag{36}$$

The source term S in the above equation represents the volumetric source generation which is equal to $\ddot{s}_{INTERCONNECT}$

$$\frac{\partial}{\partial x}\left(k \frac{\partial T}{\partial x}\right) + \frac{\partial}{\partial y}\left(k \frac{\partial T}{\partial y}\right) + \ddot{s}_{INTERCONNECT} = 0 \tag{37}$$

Integrating above equation over the control volume

$$\int_V \frac{\partial}{\partial x}\left(k\frac{\partial T}{\partial x}\right)dV + \int_V \frac{\partial}{\partial y}\left(k\frac{\partial T}{\partial y}\right)dV + \int_V SdV = 0 \tag{38}$$

Applying the Gauss Divergence Theorem,

$$\int_A \left(k\frac{\partial T}{\partial x}\right)dA + \int_V \left(k\frac{\partial T}{\partial y}\right)dA + \int_V SdV = 0 \tag{39}$$

Where,

$$\int_V SdV = \dot{s}\Delta V = \dot{s}_{INTERCONNECT}\Delta V \quad and \ \Delta V = dxdy.thk_{INTERCONNECT} \tag{40}$$

The source term can be model as below,

$$\dot{s}_{MEA} = h_{hf}A_{conv\_INTERCONNECT}(T_{hf} - T_{INTERCONNECT}) - h_{hf}A_{conv\_INTERCONNECT}(T_{INTERCONNECT} - T_{cf}) \tag{41}$$

Substituting equation (40), (41) in (39)

$$\int_s^n \left(k\frac{\partial T}{\partial x}\right)dA + \int_w^e \left(k\frac{\partial T}{\partial y}\right)dA + h_{hf}A_{conv\_INTERCONNECT}(T_{hf} - T_{INTERCONNECT}) - h_{hf}A_{conv_{INTERCONNECT}}(T_{INTERCONNECT} - T_{cf}) = 0 \tag{42}$$

which can be written as,

$$\left[kA_{c/s}\frac{\partial T}{\partial x}\right]_n - \left[kA_{c/s}\frac{\partial T}{\partial x}\right]_s + \left[kA_{c/s}\frac{\partial T}{\partial y}\right]_e - \left[kA_{c/s}\frac{\partial T}{\partial y}\right]_w + \left[\ h_{hf}A_{conv\_MEA}(T_{hf} - T_{INTERCONNECT}) - h_{cf}A_{conv\_MEA}(T_{INTERCONNECT} - T_{cf})\right] = 0 \tag{43}$$

Which can be further written as,

$$k_n A_{c/s\_n} \frac{T_N - T_P}{\Delta x} - k_s A_{c/s\_s} \frac{T_P - T_S}{\Delta x} + k_e A_{c/s\_e} \frac{T_E - T_P}{\Delta y} - k_w A_{c/s\_w} \frac{T_P - T_W}{\Delta y}$$

$$+ \left[h_{hf} A_{conv\_INTERCONNECT} \left(T_{hf} - T_P\right) \right.$$

$$\left. - h_{cf} A_{conv\_INTERCONNECT} \left(T_P - T_{cf}\right) \right] = 0 \tag{44}$$

Which can be rearranged as,

$$\left[\frac{k_n A_{c/s\_n}}{\Delta x} + \frac{k_s A_{c/s\_s}}{\Delta x} + \frac{k_e A_{c/s\_e}}{\Delta y} \right.$$

$$\left. + \frac{k_w A_{c/s\_w}}{\Delta y} + h_{hf} A_{conv\_INTERCONNECT} + h_{cf} A_{conv\_INTERCONNECT} \right] T_p$$

$$= \frac{k_n A_{c/s\_n}}{\Delta x} T_N + \frac{k_s A_{c/s\_s}}{\Delta x} T_S + \frac{k_e A_{c/s\_e}}{\Delta y} T_E + \frac{k_w A_{c/s\_w}}{\Delta y} T_W$$

$$+ h_{hf} A_{conv_{INTERCONNECT}} T_{hf} + h_{cf} A_{conv_{INTERCONNECT}} T_{cf} \tag{45}$$

Therefore, the discretized equation can be written as,

$$a_P T_P = a_N T_N + a_S T_S + a_E T_E + a_W T_W + b_{hf} T_{hf} + b_{cf} T_{cf} \tag{46}$$

Table 4.3 Coefficients for Interconnect

a_N	$\frac{k_n A_{c/s\_n}}{\Delta x}$
a_S	$\frac{k_s A_{c/s\_s}}{\Delta x}$
a_E	$\frac{k_e A_{c/s\_e}}{\Delta y}$
a_W	$\frac{k_w A_{c/s\_w}}{\Delta y}$

b_{hf}	$h_{hf}A_{conv_{INTERCONNECT}}$
b_{cf}	$h_{cf}A_{conv_{INTERCONNECT}}$
a_P	$a_N + a_S + a_E + a_W + b_{hf} + b_{cf}$

4.4 Discretization of Nodal plate

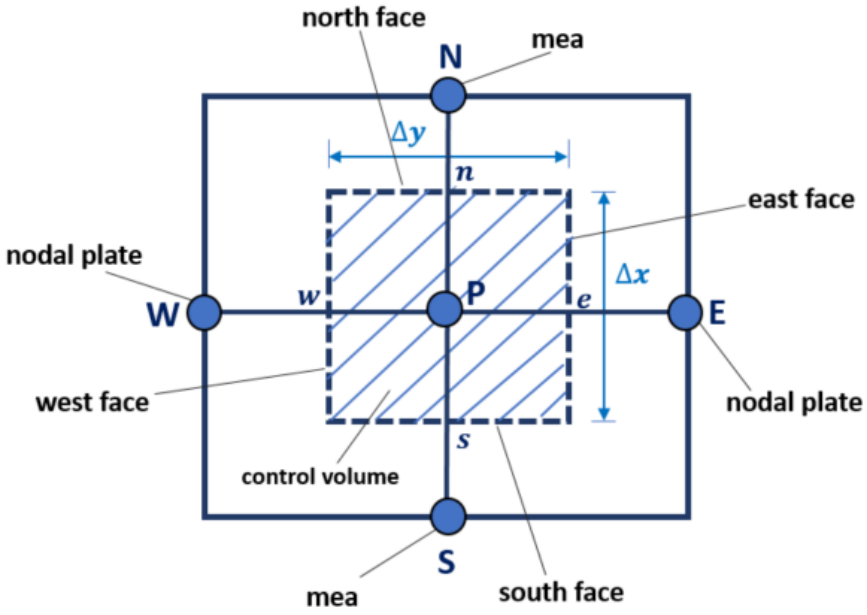

Figure 4-5 Finite volume grid for Nodal plate

Consider 2-dimensional heat conduction equation

$$\rho c \frac{\partial T}{\partial t} = \frac{\partial}{\partial x}\left(k \frac{\partial T}{\partial x}\right) + \frac{\partial}{\partial y}\left(k \frac{\partial T}{\partial y}\right) + S \tag{47}$$

The steady state form of the above equation is

$$\frac{\partial}{\partial x}\left(k \frac{\partial T}{\partial x}\right) + \frac{\partial}{\partial y}\left(k \frac{\partial T}{\partial y}\right) + S = 0 \tag{48}$$

The source term *S* in the above equation represents the volumetric source generation which is equal to $\ddot{s}_{NP}$

$$\frac{\partial}{\partial x}\left(k \frac{\partial T}{\partial x}\right) + \frac{\partial}{\partial y}\left(k \frac{\partial T}{\partial y}\right) + \ddot{s}_{NP} = 0 \tag{49}$$

Integrating above equation over the control volume

$$\int_V \frac{\partial}{\partial x}\left(k\frac{\partial T}{\partial x}\right)dV + \int_V \frac{\partial}{\partial y}\left(k\frac{\partial T}{\partial y}\right)dV + \int_V SdV = 0 \tag{50}$$

Applying the Gauss Divergence Theorem,

$$\int_A \left(k\frac{\partial T}{\partial x}\right)dA + \int_V \left(k\frac{\partial T}{\partial y}\right)dA + \int_V SdV = 0 \tag{51}$$

Where,

$$\int_V SdV = \dot{s}\Delta V = \dot{s}_{NP}\Delta V \quad and \;\; \Delta V = dxdy.thk_{NP} \tag{52}$$

The source term can be model as below,

$$\dot{s}_{NP} = \frac{k_{rib}A_{c/s\_rib}}{0.5l_{rib}}\left(T_{hot\_rib} - T_{NP}\right) - \frac{k_{rib}A_{c/s\_rib}}{0.5l_{rib}}\left(T_{NP} - T_{cold\_rib}\right) \tag{53}$$

Substituting equation (53) in (51),

$$\int_s^n \left(k\frac{\partial T}{\partial x}\right)dA + \int_w^e \left(k\frac{\partial T}{\partial y}\right)dA + \frac{k_{rib}A_{c/s\_rib}}{0.5l_{rib}}\left(T_{hot\_rib} - T_{NP}\right) - \frac{k_{rib}A_{c/s\_rib}}{0.5l_{rib}}\left(T_{NP} - T_{cold\_rib}\right) = 0 \tag{54}$$

Which can be written as,

$$\left[kA_{c/s}\frac{\partial T}{\partial x}\right]_n - \left[kA_{c/s}\frac{\partial T}{\partial x}\right]_s + \left[kA_{c/s}\frac{\partial T}{\partial y}\right]_e - \left[kA_{c/s}\frac{\partial T}{\partial y}\right]_w + \frac{k_{rib}A_{c/s\_rib}}{0.5l_{rib}}\left(T_{hot\_rib} - T_{NP}\right) - \frac{k_{rib}A_{c/s\_rib}}{0.5l_{rib}}\left(T_{NP} - T_{cold\_rib}\right) = 0 \tag{55}$$

Which further can be written as,

$$k_n A_{c/s\_n}\frac{T_N - T_P}{\Delta x} - k_s A_{c/s}\frac{T_P - T_S}{\Delta x} + k_e A_{c/s}\frac{T_E - T_P}{\Delta y} - k_w A_{c/s\_w}\frac{T_P - T_W}{\Delta y}$$

$$+\frac{k_{rib}A_{c/s\_rib}}{0.5l_{rib}}\left(T_{hot\_rib} - T_P\right) - \frac{k_{rib}A_{c/s\_rib}}{0.5l_{rib}}\left(T_P - T_{cold\_rib}\right) = 0 \tag{56}$$

which can be rearranged as,

$$\left[\frac{k_n A_{c/s\_n}}{\Delta x} + \frac{k_s A_{c/s\_s}}{\Delta x} + \frac{k_e A_{c/s\_e}}{\Delta y} + \frac{k_w A_{c/s\_w}}{\Delta y} + \frac{k_{rib}A_{c/s\_rib}}{0.5l_{rib}}\right.$$

$$\left.\frac{k_{rib}A_{c/s\_rib}}{0.5l_{rib}}\right]T_P = \frac{k_n A_{c/s\_n}}{\Delta x}T_N + \frac{k_s A_{c/s\_s}}{\Delta x}T_S + \frac{k_e A_{c/s\_e}}{\Delta y}T_E$$

$$+\frac{k_w A_{c/s\_w}}{\Delta y}T_W + \frac{k_{rib}A_{c/s\_rib}}{0.5l_{rib}}T_{hot\_rib}$$

$$+\frac{k_{rib}A_{c/s\_rib}}{0.5l_{rib}}T_{cold\_rib} \tag{57}$$

Therefore, the discretized equation can be written as,

$$a_P T_P = a_N T_N + a_S T_S + a_E T_E + a_W T_W + b_{hot\_rib}T_{hot\_rib} + b_{cold\_rib}T_{cold\_rib} \tag{58}$$

Table 4.4 Coefficients for Nodal plate

a_N	$\frac{k_n A_{c/s\_n}}{\Delta x}$
a_S	$\frac{k_s A_{c/s\_s}}{\Delta x}$
a_E	$\frac{k_e A_{c/s\_e}}{\Delta y}$
a_W	$\frac{k_w A_{c/s\_w}}{\Delta y}$

b_{hot_rib}	$\frac{k_{rib}A_{c/s\_rib}}{0.5l_{rib}}$
b_{cold_rib}	$\frac{k_{rib}A_{c/s\_rib}}{0.5l_{rib}}$
a_P	$a_P = a_N + a_S + a_E + a_W + b_{hot\_rib} + b_{cold\_rib}$

4.5 Discretization of the Rib

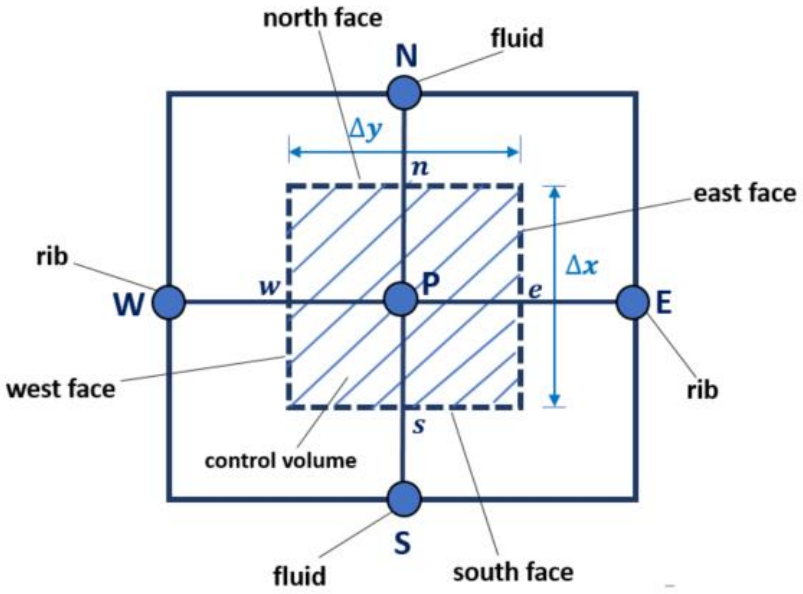

Figure 4-6 Finite volume grid for Rib

Consider 1-dimensional heat conduction equation

$$\rho c \frac{\partial T}{\partial t} = \frac{\partial}{\partial y}\left(k \frac{\partial T}{\partial y}\right) + S \tag{59}$$

The steady state form of the above equation is

$$\frac{\partial}{\partial y}\left(k \frac{\partial T}{\partial y}\right) + S = 0 \tag{60}$$

The source term *S* in the above equation represents the volumetric source generation which is equal to $\ddot{s}_{rib}$.

$$\frac{\partial}{\partial y}\left(k \frac{\partial T}{\partial y}\right) + \ddot{s}_{rib} = 0 \tag{61}$$

Integrating above equation over the control volume

$$\int_V \frac{\partial}{\partial y}\left(k\frac{\partial T}{\partial y}\right)dV + \int_V SdV = 0 \tag{62}$$

Applying the Gauss Divergence Theorem,

$$\int_A \left(k\frac{\partial T}{\partial y}\right)dA + \int_V SdV = 0 \tag{63}$$

`

Where,

$$\int_V SdV = \dot{s}\Delta V = \dot{s}_{rib}\Delta V \quad and \;\; \Delta V = dxdy.thk_{rib} \tag{64}$$

The source term can be model as below,

$$\begin{aligned}\dot{s}_{rib} = {} & h_{fluid}\,A_{conv\_rib}\left(T_{fluid\_R} - T_{rib}\right) + h_{fluid}\,A_{conv\_rib}\left(T_{fluid\_L} - T_{rib}\right) \\ & -\frac{k_{rib}A_{c/s\_rib}}{0.5l_{rib}}\left(T_{rib} - T_{NP\_1}\right) - \frac{k_{rib}A_{c/s\_rib}}{0.5l_{rib}}\left(T_{rib} - T_{NP\_2}\right) \\ & -q_{SR\_\&\_WGS} + \Delta h_{f\_SR}n_{CH_4}\big|_{SR} + \Delta h_{f\_WGS}n_{CO}|_{WGS}\end{aligned} \tag{65}$$

Where,

$$\begin{aligned}q_{SR\_\&\_WGS} = {} & \\ & -T_{fluid\_R}\left(n_{CH_4}\big|_{SR}C_{p\_CH_4} + n_{H_2O}\big|_{SR}C_{p\_H_2O} + n_{CO}|_{WGS}C_{p\_Co} + n_{H_2O}\big|_{WGS}C_{p\_H_2O}\right) \\ & -T_{fluid\_L}\left(n_{CH_4}\big|_{SR}C_{p\_CH_4} + n_{H_2O}\big|_{SR}C_{p\_H_2O} + n_{CO}|_{WGS}C_{p\_Co} + n_{H_2O}\big|_{WGS}C_{p\_H_2O}\right) \\ & +T_{rib}\left(n_{CO}|_{SR}C_{p\_CO} + 3\,n_{H_2}\big|_{SR}C_{p\_H_2} + n_{CO_2}\big|_{WGS}C_{p\_CO_2} + n_{H_2}\big|_{WGS}C_{p\_H_2}\right)\end{aligned} \tag{66}$$

Substituting equation (64), (65) in (63)

$$\int_w^e \left(k\frac{\partial T}{\partial y}\right) dA + h_{fluid}\, A_{conv\_rib}\left(T_{fluid\_R} - T_{rib}\right)$$

$$+ h_{fluid}\, A_{conv\_rib}\left(T_{fluid\_L} - T_{rib}\right) - \frac{k_{rib}A_{c/s\_rib}}{0.5l_{rib}}\left(T_{rib} - T_{NP\_1}\right)$$

$$-\frac{k_{rib}A_{c/s\_rib}}{0.5l_{rib}}\left(T_{rib} - T_{NP\_2}\right) - q_{SR\_\&\_WGS} + \left.\Delta h_{f_{SR}} n_{CH_4}\right|_{SR}$$

$$+ \Delta h_{f_{WGS}} n_{CO}|_{WGS} = 0 \tag{67}$$

Which can be written as,

$$\left[kA_{c/s\_rib}\frac{\partial T}{\partial y}\right]_e - \left[kA_{c/s\_rib}\frac{\partial T}{\partial y}\right]_w + h_{fluid}\, A_{conv\_rib}\left(T_{fluid\_R} - T_P\right)$$

$$+ h_{fluid}\, A_{conv\_rib}\left(T_{fluid\_L} - T_P\right) - \frac{k_{rib}A_{c/s\_rib}}{0.5l_{rib}}\left(T_P - T_{NP\_1}\right)$$

$$-\frac{k_{rib}A_{c/s\_rib}}{0.5l_{rib}}\left(T_P - T_{NP\_2}\right) - q_{SR\_\&\_WGS} + \left.\Delta h_{f_{SR}} n_{CH_4}\right|_{SR}$$

$$+ \Delta h_{f_{WGS}} n_{CO}|_{WGS} = 0 \tag{68}$$

Which can be further written as,

$$k_e A_{c/s\_rib}\frac{T_E - T_P}{\Delta y} - k_w A_{c/s\_rib}\frac{T_P - T_W}{\Delta y} + h_{fluid}\, A_{conv\_rib}\left(T_{fluid\_R} - T_P\right)$$

$$+ h_{fluid}\, A_{conv\_rib}\left(T_{fluid\_L} - T_P\right) - \frac{k_{rib}A_{c/s\_rib}}{0.5l_{rib}}\left(T_P - T_{NP\_1}\right)$$

$$-\frac{k_{rib}A_{c/s\_rib}}{0.5l_{rib}}\left(T_P - T_{NP\_2}\right) - q_{SR\_\&\_WGS} + \left.\Delta h_{f_{SR}} n_{CH_4}\right|_{SR}$$

$$+\Delta h_{f_{WGS}} n_{CO}|_{WGS} = 0 \tag{69}$$

Substituting (66) in (69),

$$k_e A_{c/s\_rib}\frac{T_E - T_P}{\Delta y} - k_w A_{c/s\_rib}\frac{T_P - T_W}{\Delta y} + h_{fluid}\,A_{conv\_rib}\left(T_{fluid\_R} - T_P\right)$$

$$+ h_{fluid}\,A_{conv\_rib}\left(T_{fluid\_L} - T_P\right) - \frac{k_{rib}A_{c/s\_rib}}{0.5 l_{rib}}\left(T_P - T_{NP\_1}\right)$$

$$- \frac{k_{rib}A_{c/s\_rib}}{0.5 l_{rib}}\left(T_P - T_{NP_2}\right) + \Delta h_{f_{SR}} n_{CH_4}\big|_{SR} + \Delta h_{f_{WGS}} n_{CO}|_{WGS}$$

$$+ T_{fluid\_R}\left(n_{CH_4}\big|_{SR} C_{p\_CH_4} + n_{H_2O}\big|_{SR} C_{p\_H_2O} + n_{CO}|_{WGS} C_{p\_Co} + n_{H_2O}\big|_{WGS} C_{p\_H_2O}\right)$$

$$+ T_{fluid\_L}\left(n_{CH_4}\big|_{SR} C_{p\_CH_4} + n_{H_2O}\big|_{SR} C_{p\_H_2O} + n_{CO}|_{WGS} C_{p\_Co} + n_{H_2O}\big|_{WGS} C_{p\_H_2O}\right)$$

$$- T_P\left(n_{CO}|_{SR} C_{p\_CO} + 3\,n_{H_2}\big|_{SR} C_{p\_H_2} + n_{CO_2}\big|_{WGS} C_{p\_CO_2} + n_{H_2}\big|_{WGS} C_{p\_H_2}\right) = 0 \quad (70)$$

Which can be rearranged as,

$$\left[\frac{k_e A_{c/s\_rib}}{\Delta y} + \frac{k_w A_{c/s\_rib}}{\Delta y} + h_{fluid}\,A_{conv\_rib} + h_{fluid}\,A_{conv\_rib} + \frac{k_{rib}A_{c/s\_rib}}{0.5 l_{rib}}\right.$$

$$\left(n_{CO}|_{SR} C_{p\_CO} + 3\,n_{H_2}\big|_{SR} C_{p\_H_2} + n_{CO_2}\big|_{WGS} C_{p\_CO_2} + n_{H_2}\big|_{WGS} C_{p\_H_2}\right)$$

$$\left. + \frac{k_{rib}A_{c/s\_rib}}{0.5 l_{rib}}\right] T_P = \frac{k_e A_{c/s\_rib}}{\Delta y} T_E + \frac{k_w A_{c/s\_rib}}{\Delta y} T_W + \left(h_{fluid}\,A_{conv\_rib}\right.$$

$$\left. + n_{CH_4}\big|_{SR} C_{p_{\_CH_4}} + n_{H_2O}\big|_{SR} C_{p_{\_H_2O}} + n_{CO}|_{WGS} C_{p_{\_Co}} + n_{H_2O}\big|_{WGS} C_{p_{\_H_2O}}\right) T_{fluid\_R}$$

$$+ \left(h_{fluid}\,A_{conv\_rib} + n_{CH_4}\big|_{SR} C_{p\_CH_4} + n_{H_2O}\big|_{SR} C_{p\_H_2O} + n_{CO}|_{WGS} C_{p\_Co}\right.$$

$$\left. + n_{H_2O}\big|_{WGS} C_{p_{\_H_2O}}\right) T_{fluid\_L} + \frac{k_{rib}A_{c/s\_rib}}{0.5 l_{rib}} T_{NP\_1} + \frac{k_{rib}A_{c/s\_rib}}{0.5 l_{rib}} T_{NP\_2}$$

$$+ \Delta h_{f_{SR}} n_{CH_4}\big|_{SR} + \Delta h_{f_{WGS}} n_{CO}|_{WGS} \quad (71)$$

Therefore, the discretized equation can be written as,

$$a_P T_P = a_E T_E + a_W T_W + b_{fluid\_R} T_{fluid\_R} + b_{fluid\_L} T_{fluid\_L} + b_{NP\_1} T_{NP\_1} + b_{NP\_2} T_{NP\_2} + B \quad (72)$$

Table 4.5 Coefficients for Rib

a_E	$\frac{k_e A_{c/s\_rib}}{\Delta y}$
a_W	$\frac{k_w A_{c/s\_rib}}{\Delta y}$
b_{fluid_R}	$h_{fluid} A_{conv\_rib} + n_{CH_4}\big\vert_{SR} C_{p\_CH_4} + n_{H_2O}\big\vert_{SR} C_{p\_H_2O} + n_{CO}\vert_{WGS} C_{p\_Co} + n_{H_2O}\big\vert_{WGS} C_{p\_H_2O}$
b_{fluid_L}	$h_{fluid} A_{conv\_rib} + n_{CH_4}\big\vert_{SR} C_{p\_CH_4} + n_{H_2O}\big\vert_{SR} C_{p\_H_2O} + n_{CO}\vert_{WGS} C_{p\_Co} + n_{H_2O}\big\vert_{WGS} C_{p\_H_2O}$
b_{NP_1}	$\frac{k_{rib} A_{c/s\_rib}}{0.5 l_{rib}}$
b_{NP_2}	$\frac{k_{rib} A_{c/s\_rib}}{0.5 l_{rib}}$
B	$\Delta h_{f_{SR}} n_{CH_4}\big\vert_{SR} + \Delta h_{f_{WGS}} n_{CO}\vert_{WGS}$
a_P	$a_E + a_W + b_{fluid\_R} + b_{fluid\_L} + b_{NP\_1} + + b_{NP\_2} + B$

Chapter 5

VALIDATION AND RESULTS

To analyze the performance of the planar stack the model was simulated for two cases

Case 1: Simulation when working fluid at both cathode and anode is air.

Case 2: Simulation when working fluid at cathode is air and gas mixture at anode (reformer model).

Case 1: Simulation when working fluids at cathode and anode is air.

To validate the model, the Effectiveness is calculated for different length and the solution obtained from solver and from analytical solution is compared.

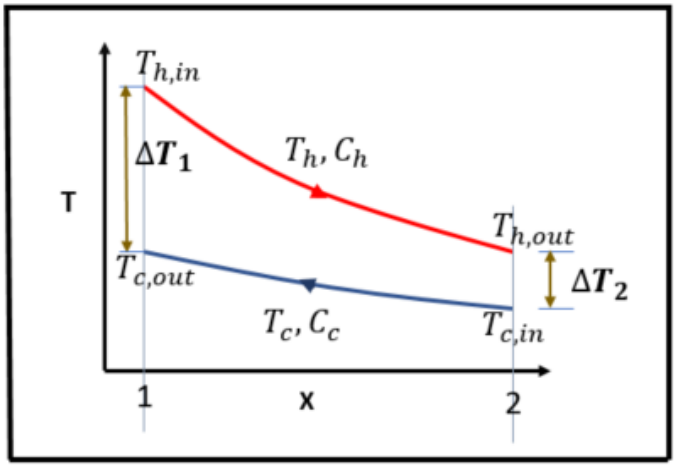

Figure 5-1 Temperature profile for counter-flow arrangement

Effectiveness calculated by the solver

The actual effectiveness is calculated using,

$$Effectiveness\ (\varepsilon) = \frac{q}{q_{max}}$$

Where, $q_{\max}$ represent maximum heat transfer possible.

$$q_{max} = C_{min}(T_{h,i} - T_{c,i})$$

$C_{\min}$ is the smallest value among C_h or C_c. This is indicative that the fluid having the smallest specific heat would undergo a highest heat transfer. 'q' is the actual heat transfer based on cold or hot fluid whichever is of Interest [23].

$$q = C_c(T_{c,o} - T_{c,i}) \qquad (cold\ fluid)$$

$$q = C_h(T_{h,i} - T_{h,o}) \qquad (hot\ fluid)$$

Effectiveness calculated using analytical solution

The analytical / theoretical solution is calculated using Effectiveness-NTU method. This method works under the assumptions that there is no axial conduction, no heat leakage, and no considerable variations in properties along the flow direction [23]. The following equations are used to calculate effectiveness analytically.

$$\varepsilon = \frac{1 - exp[-NTU(1 - C_r)]}{1 - C_r exp[-NTU(1 - C_r)]} \quad if\ (C_r < 1)$$

$$\varepsilon = \frac{NTU}{1 + NTU} \quad if(C_r = 1)$$

Simulations are performed for the model of dimension as per [21] and effectiveness obtained from solver and the analytical method is compared.

case (a): Height of the cathode channel = 2 mm

Height of the anode channel = 1 mm

Width of the channels = 8 mm

Thickness of the MEA = 0.28 mm

Thickness of the interconnect =1 mm

Thickness of the rib = 2 mm

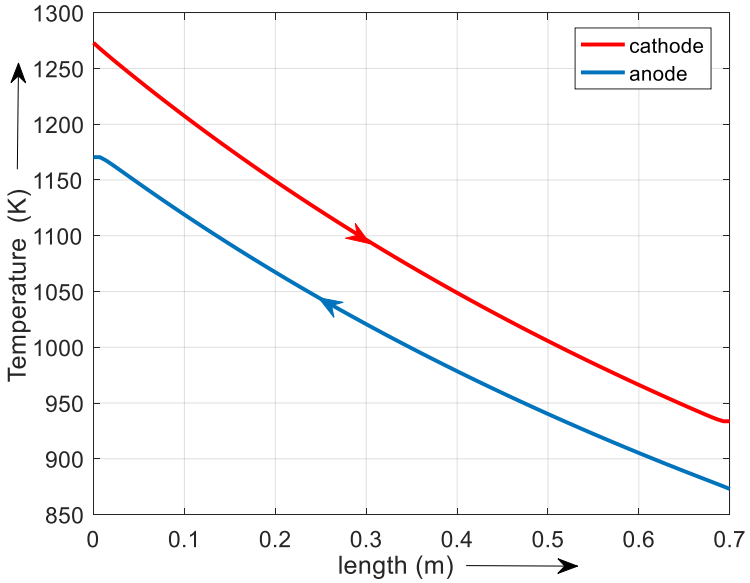

Figure 5-2 Temperature plot for cathode and anode fluid temperature for case (a)

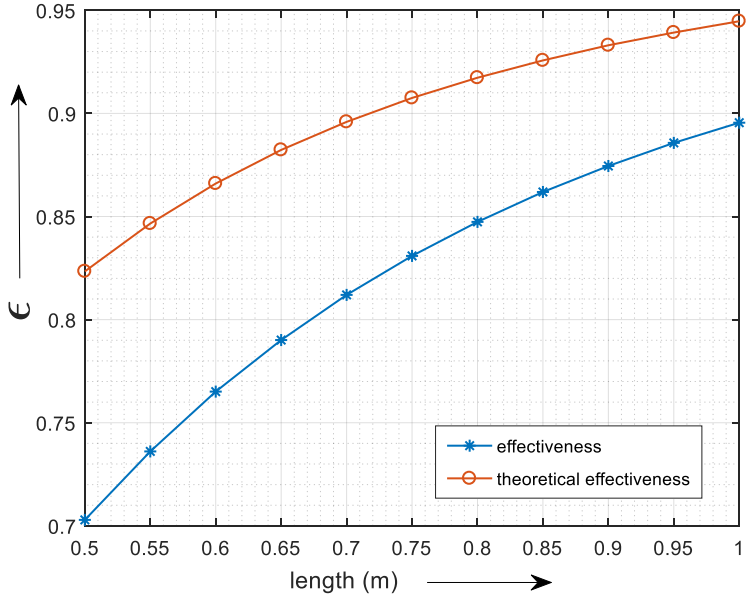

Figure 5-3 Comparing effectiveness obtained from the solver and theoretical effectiveness for case (a)

case (b): Height of the cathode channel = 2 mm

Height of the anode channel = 1 mm

Width of the channels = 5mm

Thickness of the MEA = 0.28 mm

Thickness of the interconnect =1 mm

Thickness of the rib = 2mm

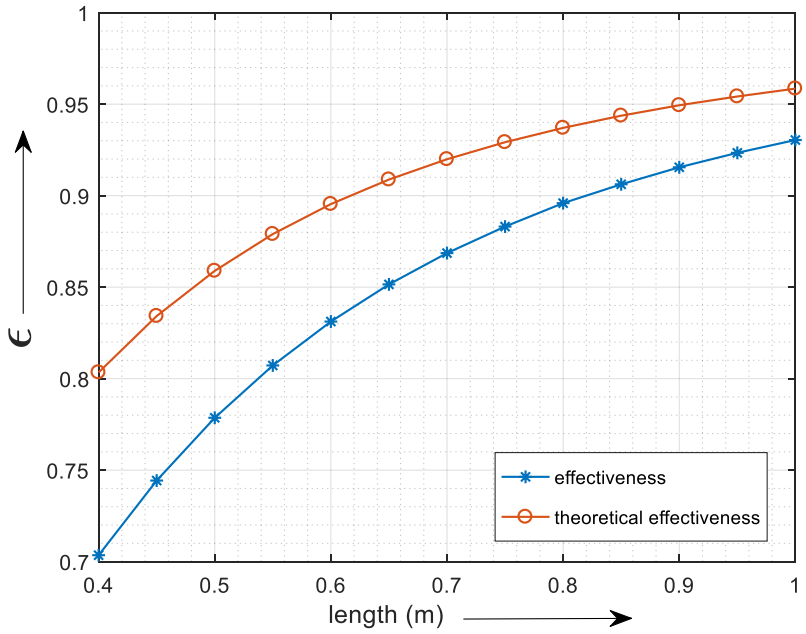

Figure 5-4 Comparing effectiveness obtained from the solver and theoretical effectiveness for case (b)

Thus, from the Figure 5-3 and Figure 5-4 it is clear that the effectiveness increases with the length of the model. Typically for the heat exchanging model an effectiveness greater than 0.85 is desired. For case(a), An Effectiveness greater than 0.85 is obtained for a length of 0.85 m and above. However, running the same case by changing the width of the channel to 0.005m as in case(b) the same effectiveness is obtained for length of 0.7 m.

Since all the other dimension parameters mentioned above are fixed, the only possible parameter's that can be tweaked is the length or the width of the model. Moreover, compactness of the model is of importance when is applicability is concern. As a result, there is a trade-off while selecting length and width for the model to be compact.

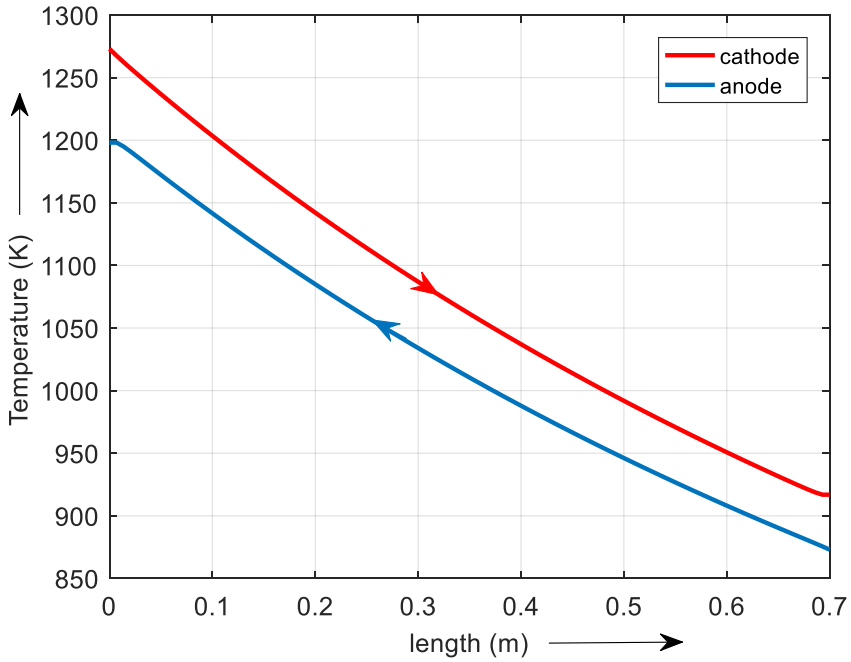

Figure 5-5 Temperature plot for cathode and anode fluid temperature for case (b)

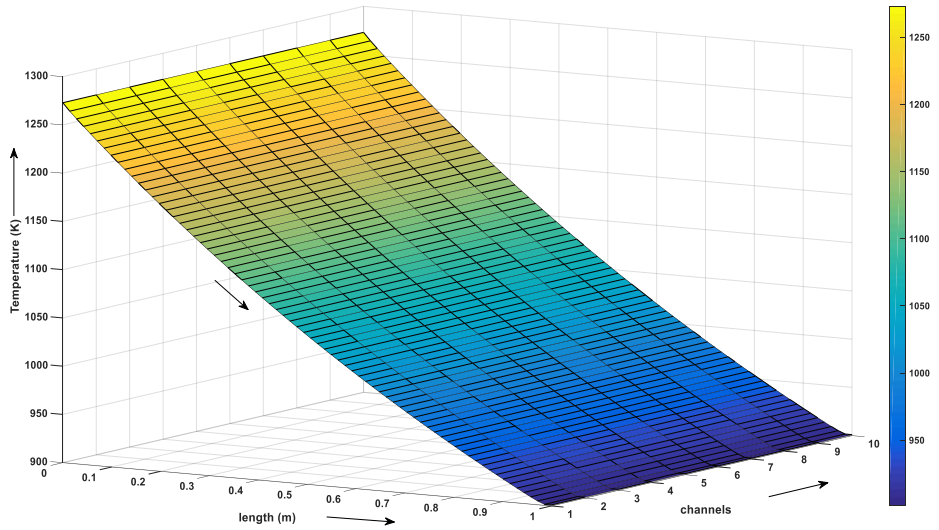

Figure 5-6 Cathode fluid temperature for case (b)

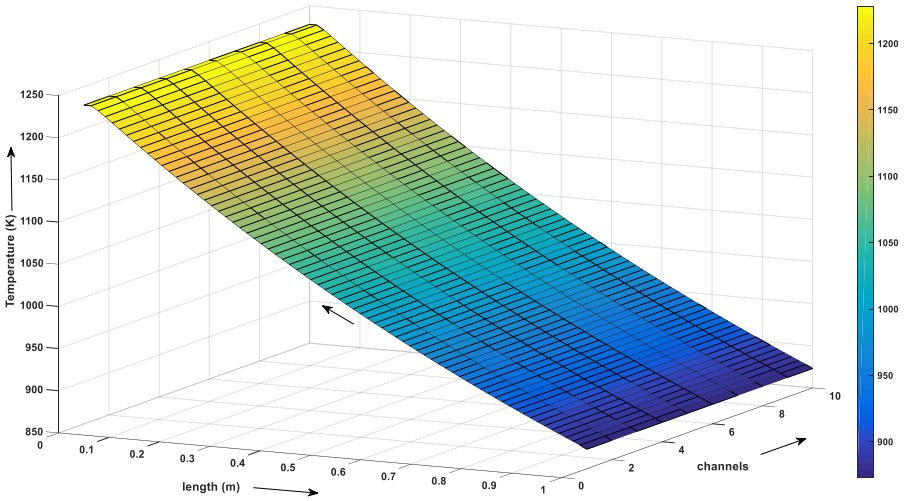

Figure 5-7 Anode fluid temperature for case (b)

Case 2: Simulation when working fluid at cathode is air and gas mixture at anode (reformer model)

As indicated the scope of the present work is to simulate the steady state characteristic of the SOFC stack undergoing internal reforming. The stack model is a reactor where hot air at high temperature enters the cathode, and the gas mixture at anode and undergoes reaction due to heat received from the hot air. Hot air is also supplied initially before feeding the mixture to heat the stack at desired temperature. The mixture should also, be preheated to initiate the reaction as soon as it enters the channel. A suitable steam to carbon ratio (SCR) of around 2 to 2.5 at the inlet is required to avoid the circumstances mentioned before. SCR at the inlet is calculated as,

$$SCR = \frac{n|_{H_2O}}{n|_{CH_4}}$$

While the molar flux (mol/s) at inlet for the fuel and steam is calculated as,

$$n|_{CH_4} = \frac{MW_{CH_4}}{\left(y_{CH_4}MW_{CH_4} + y_{H_2O}MW_{H_2O}\right)} y_{CH_4}\dot{m}$$

$$n|_{H_2O} = \frac{MW_{H_2O}}{\left(y_{CH_4}MW_{CH_4} + y_{H_2O}MW_{H_2O}\right)} y_{H_2O}\dot{m}$$

Simulations were performed for the SCR = 2 and SCR = 2.5 and the corresponding mole fractions for steam and methane are supplied at the entry for the mixture. Also, the operating temperature for both air and gas mixture is changed to study the effects of operating temperature on mixture concentration.

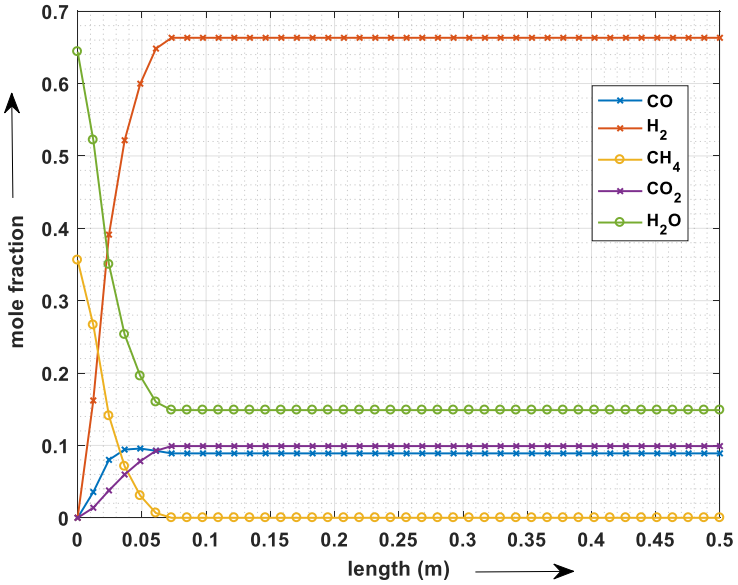

Figure 5-8 Mole fraction for species, SCR=2, air inlet temperature = 1000K and mixture inlet temperature = 900 K

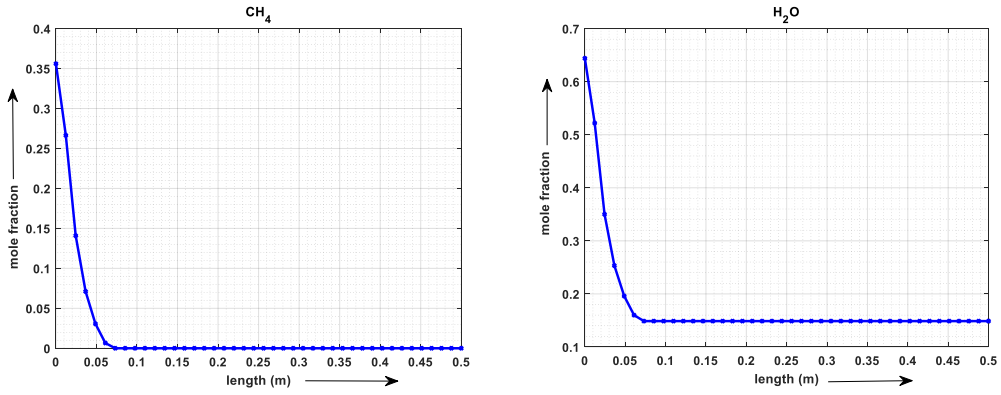

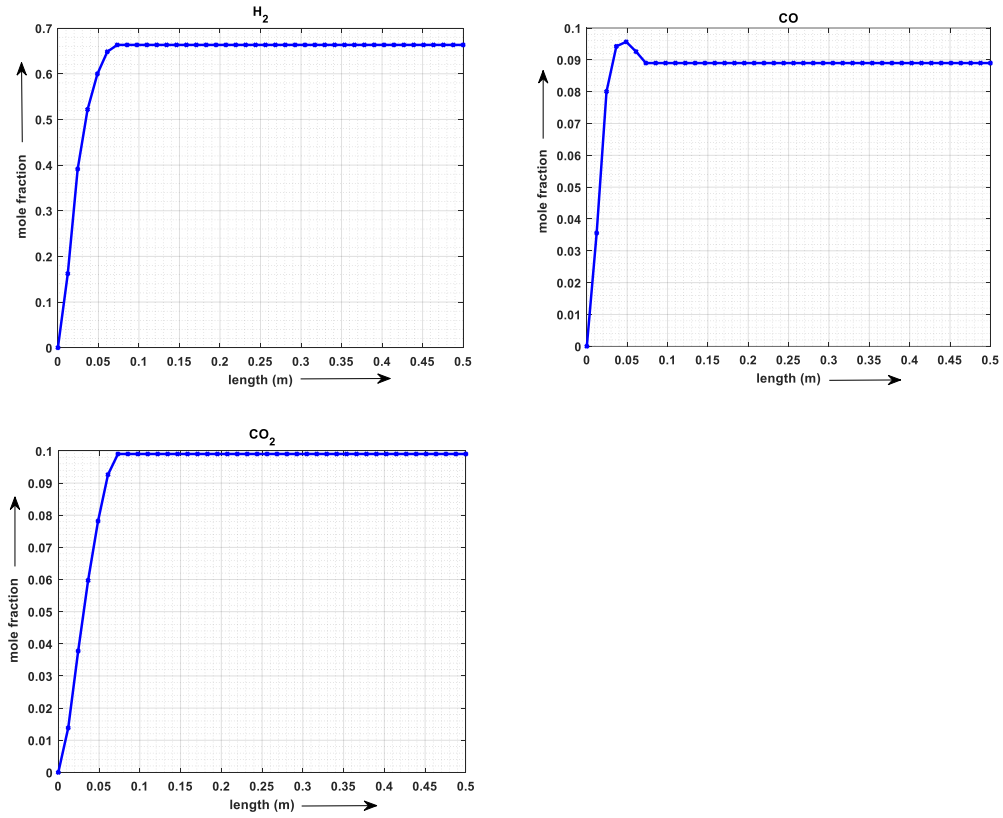

Figure 5-9 Individual species mole fraction, SCR=2, air inlet temperature=1000 K and mixture inlet temperature = 900 K

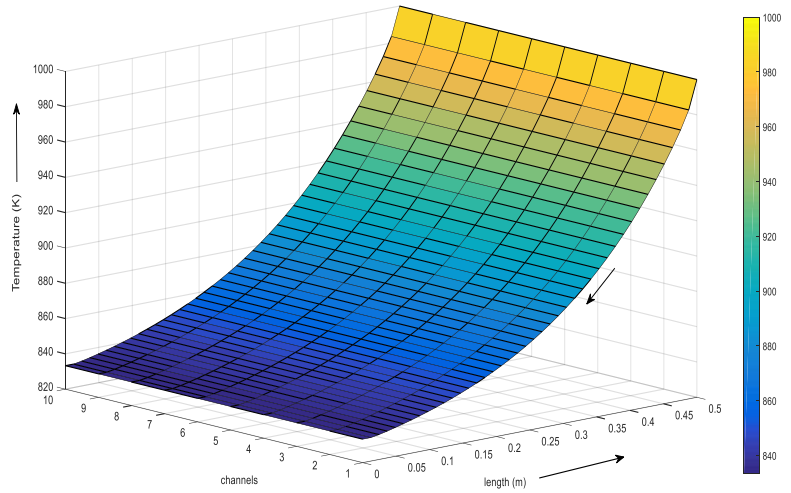

Figure 5-10 Temperature plot for air at cathode, SCR=2, air inlet temperature = 1000 K, mixture inlet temperature = 900 K

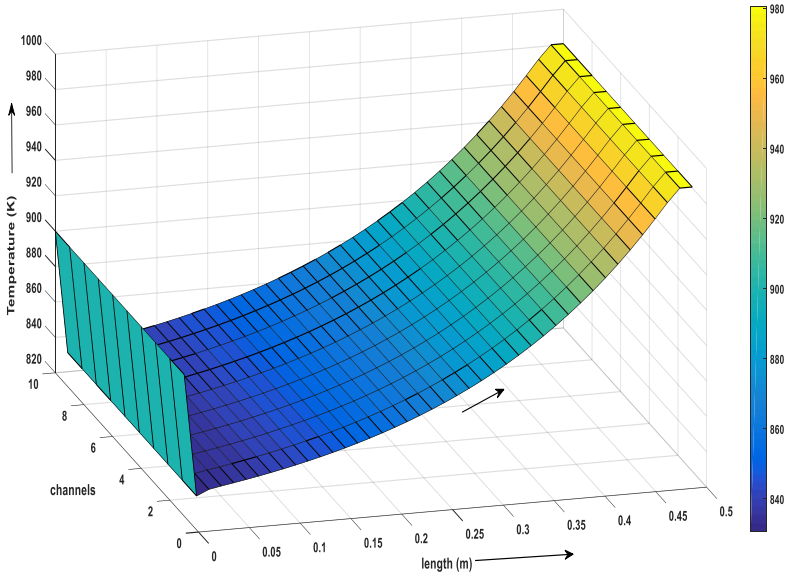

Figure 5-11 Temperature plot for mixture at anode, SCR=2, air inlet temperature = 1000K mixture inlet temperature = 900 K

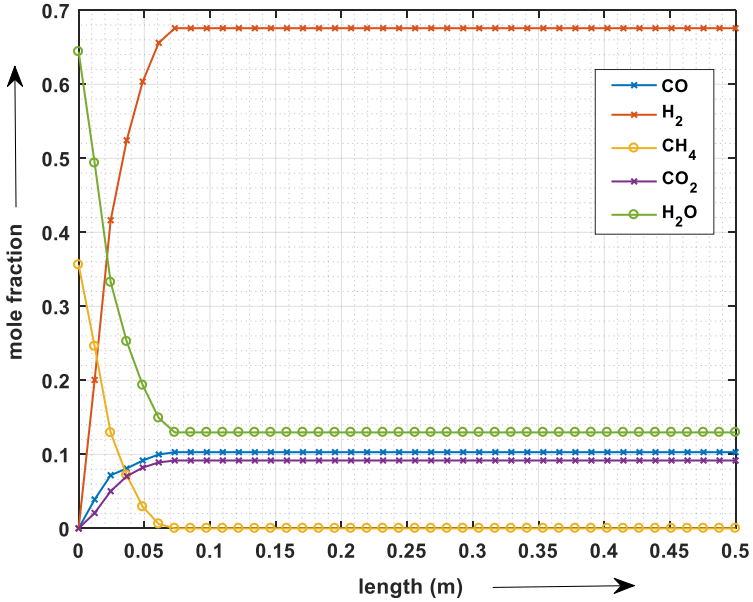

Figure 5-12 Mole fraction for species SCR=2, air inlet temperature =1125K and mixture inlet temperature = 925 K

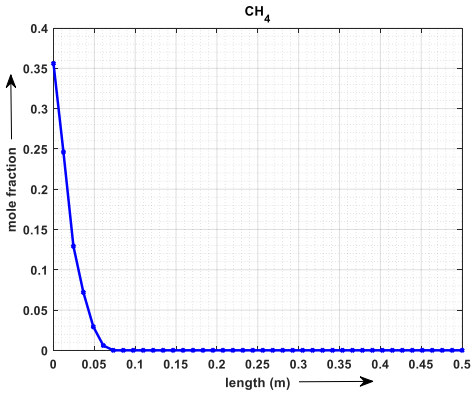

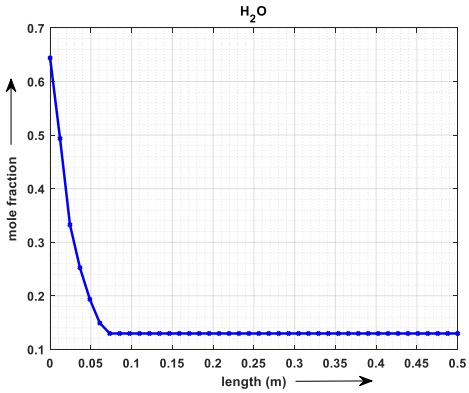

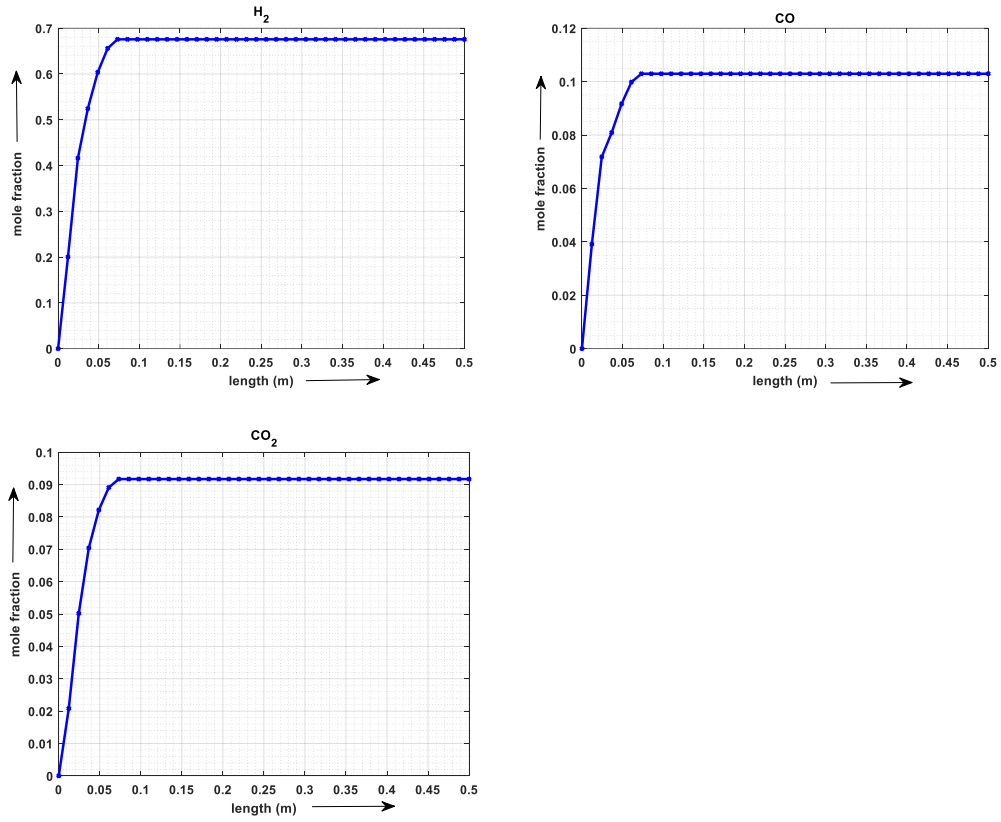

Figure 5-13 Individual Species mole fraction, SCR=2, air inlet temperature = 1125 and mixture inlet temperature = 925 K

As can be seen from the Figure 5-8 - Figure 5-13, A soon as the mixture enters the anode channel, both the SR and WGS reaction occur instantly, the number of moles of methane, water decrease rapidly and hence hydrogen, carbon dioxide and carbon monoxide are obtained as the product. Also, the reaction completes rapidly this mainly accounts to the low flow rate of the mixture entering the anode and high reaction rate which results in fast conversion of reactants to product. The effect of high operating temperature can be seen in the Figure 5-8 and Figure 5-12 which shows higher concentration of hydrogen and carbon monoxide at the outlet in Figure 5-12 compared to Figure 5-8.

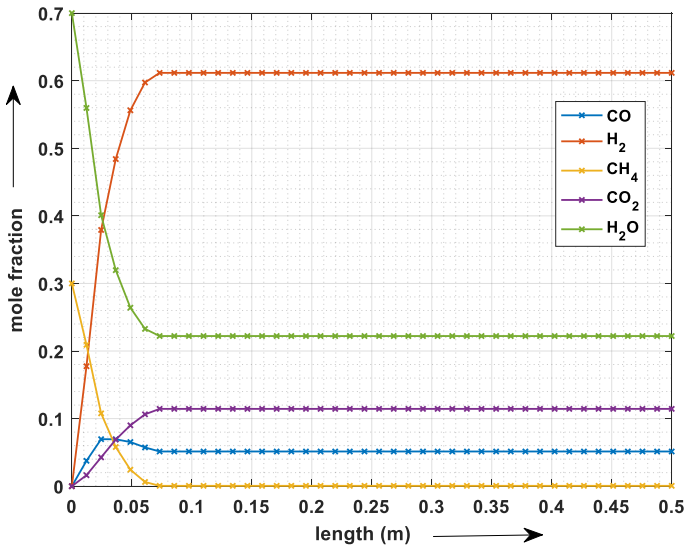

Figure 5-14 Mole fraction for species SCR=2.5, air inlet temperature = 1000 K and mixture inlet temperature = 900 K

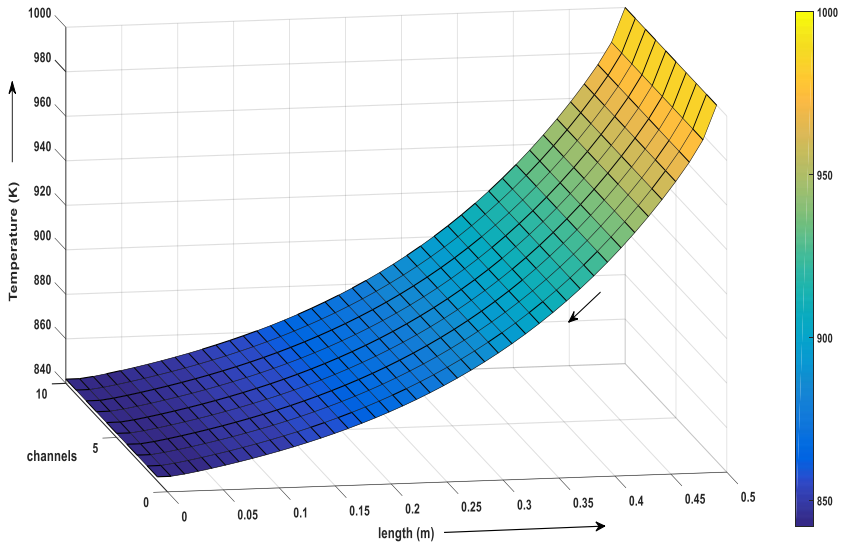

Figure 5-15 Temperature plot for air at cathode, SCR=2.5, air inlet temperature = 1000 K, mixture inlet temperature = 900 K

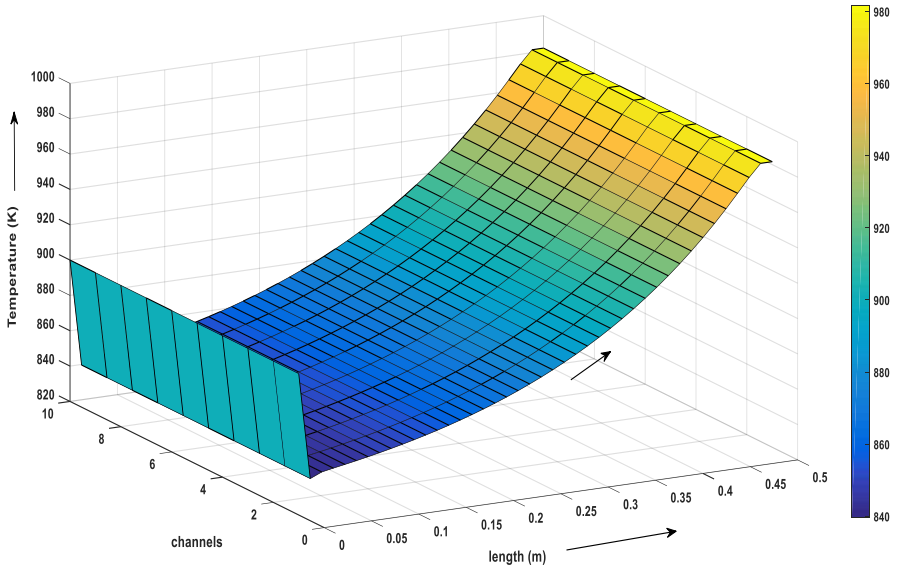

Figure 5-16 Temperature plot for mixture at anode, SCR=2.5, air inlet temperature = 1000 K, mixture inlet temperature = 900 K

Also, the effect of varying SCR was studied, Figure 5-8 and Figure 5-14 show that the number of mole of hydrogen formed at SCR = 2 is greater than that for SCR = 2.5 at the same operating temperature. As a result, the lower SCR shows a high yield in hydrogen formation and hence better performance. This is due to dilution of hydrogen by steam at higher SCR.

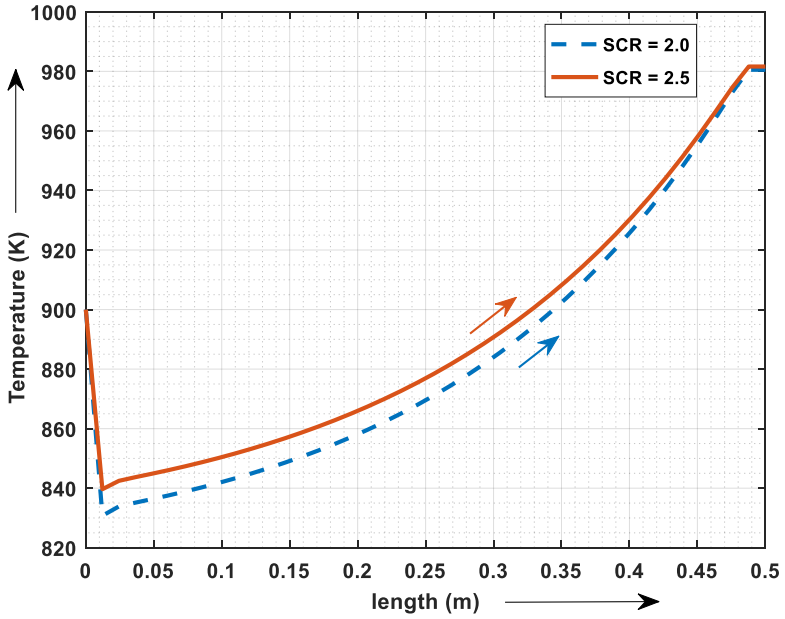

Figure 5-17 Comparing cathode mixture temperature for SCR = 2 and SCR = 2.5, air inlet temperature = 1000, mixture inlet temperature = 900 K

It can be seen from the Figure 5-17, there is sudden drop in mixture temperature at the anode inlet. This is due to the endothermic nature of the combined SR and WGS reactions and soon the mixture temperature increases gradually by absorbing heat from the hot air. Also, it can be seen from figure 5-17 that larger SCR results in higher mixture temperature at the exit this is due to the presence of higher mole fraction of steam at exit which carries a large thermal energy.

Chapter 6

CONCLUSION

The thesis presents a numerical heat transfer model of planar SOFC stack, working as a reformer. The finite volume discretization method is used to discretize the domain under consideration and solve for the mass flow rate, temperature for both fluid and solid structure. Boundary conditions in terms Pressure at inlet and outlet and Temperature at the inlets are provided for fluid domain to solve the momentum and energy equation. The property variations like specific heat, conductivity, viscosity etc. are modelled along the flow direction as a function of temperature. Species concentration at the inlet is provided to solve the species conservation equation. Reaction kinetics like rate constant, equilibrium constant, Gibbs function etc. which are modelled as a function of temperature are used to calculate the species variations in the mixture. The steady state form of convection-diffusion equation is used to solve temperature for air and gas mixture and the steady state conduction equation for solid hardware.

The developed solver can be easily tweaked thus making it work for wide range of fluids, for different hardware dimensions as well as under different values for temperature and pressure at the boundaries. For example, if we know the operating temperature, pressure, and the working fluid, we can easily calculate the properties of the fluid using regression values from available data sources or if we need to change the channel dimensions and cross-section we can easily alter the geometry by changing the dimension parameters. Pressure values at the inlet and the outlet can be assigned and thus the required pressure drop can be obtained along the flow.

The solver can be used as a tool to predict the performance of the model prior to building a prototype thus providing information required during design considerations as a result saving cost and time. It can also be used to validate an existing model by altering the solver parameters as mentioned above. It can be easily integrated into a complex cycle like the Gas Turbine cycle or can be used a stand-alone model to analyze and validate the model at the component level.

Chapter 7

SCOPE OF FUTURE WORK

I. In the present research only one unit consisting of anode, cathode is simulated, the model can be scaled to compute multiple channels and stacks thus following more realistic approach.

II. The circuit model can be easily implemented to simulate the current and voltage characteristic which is prime objective of planar stack.

III. Heat loss due to radiation, leakage and to environment can be model to understand the effects of more realistic conditions on the working of the model.

IV. The model can be easily integrated into a cycle and thus an entire cycle can be simulated by understanding the detail working and effectiveness at the component level thus evaluating the overall cycle efficiency.

V. A more realistic approach is analyzing the model under transient condition, as a result the time dependent effects need to be considered thus solving all the governing equation in their transient form.

REFERENCES

[1] Integrated modelling approach for solid oxide fuel cell – based power generating system, Jeongpill Ki

[2] Operating characteristic of a 5kW class anode-supported planar SOFC stack for a fuel cell/ gas turbine hybrid system, Tak-Hyoung Lim, Rak-Hyun Song, Dong-Ryul Shin, Jung-Il Yang, Heon Jung, I.C. Vinke, Soo-Seok Yang

[3] On the effect of methane internal reforming modelling in solid oxide fuel cells, D.Sanchez, R. Chacartegui, A. Munoz, T. Sanchez

[4] Solid Oxide Fuel cells: An Overview, S.C. Singhal

[5] Thermodynamic and transport properties of gases for use in solid oxide fuel cell modelling, B. Todd, J.B. Young

[6] Transport Phenomenon, R. Byron Bird, Warren E. Stewart, Edwin N. Lightfoot

[7] A Thermodynamic Analysis of Tubular Solid Oxide Fuel Cell Based Hybrid Systems, A.D. Rao , G.S. Samuelsen

[8] Simplified Versus Detailed SOFC Reactor Models and Influence on the Simulation of the Design Point Performance of Hybrid Systems, Loredana Magistri, Riccardo Bozzo, Paola Costamagna and Aristide F. Massardo

[9] Modelling of simple hybrid solid oxide fuel cell and gas turbine power plant, S.H. Chan, H.K. Ho, Y.Tian

[11] Modeling of Solid Oxide Heat Exchanger Integrated Stack and Simulation at High

Fuel Utilization, Paola Costamagna and Kaspar Honegger

[12] Synergistic integration of a gas turbine and solid oxide fuel cell for improved transient capability, Fabian Mueller, Robert Gaynor, Allie E. Auld, Jacob Brouwer, Faryar Jabbari, G. Scott Samuelsen.

[13] Dynamic modelling of single tubular SOFC combining heat/mass transfer and electrochemical reaction effects, X.Xue, J. Tang, N. Sammes, Y. Du

[14] Three-dimensional thermos-fluid electrochemical modelling of planar SOFC stack, K.P. Recnagle, R.E. Williford, L.A. Chick, D.R. Rector, M.A. Khaleel

[15] Simulation of the chemical/electrochemical reactions and heat/mass transfer for a tubular SOFC in a stack, Pei-Wen Li, Minking K. Chyu

[16] A numerical study of cell-to-cell variations in a SOFC stack, A.C. Burt, I.B. Celik, R.S. Gemmen, A.V. Smirnov

[17] A heat exchanger model that includes axial conduction, parasitic heat loads and property variations, G.F. Nellis

[18] Computational model for steady state simulation of a plate-fin heat exchanger, Ajit Rajesh Desai

[19] Computational model for transient and steady state analysis of a 1-Dimensional Auto-Thermal reformer, Srikanth Honavara-Prasad

[20] Investigation of harmonic instability of laminar flow past 2D rectangular cross section with 0.5-4 aspect ratios, Behzad Ghadiri Dehkordi, Saleh Fallah, Amirreza Niazmand

[21] Computational model to predict thermal dynamics of planar solid oxide fuel cell stack during start-up process, Jeongpill Ki, Daejong Kim

[22] Computational Fluid Dynamic Modelling of Solid Oxide Fuel Cell Stacks, Robert Takeo Nishida

[23] Incropera, F.P., Dewitt, D.P. Fundamentals of Heat Transfer 2nd ed. John Wiley, New York, 1985

BIOGRAPHICAL INFORMATION

Vaibhav Indulkar earned his Bachelor in Mechanical Engineering from University of Mumbai, India in 2014. He joined University of Texas at Arlington to pursue his Master of Science in Mechanical Engineering in Fall 2015. He worked at Turbomachinery and Energy System Laboratory during his graduate studies and carried out his research in field of thermal and fluid science. His research interest includes numerical modelling of heat transfer and fluid flow, computational fluid dynamics.

.